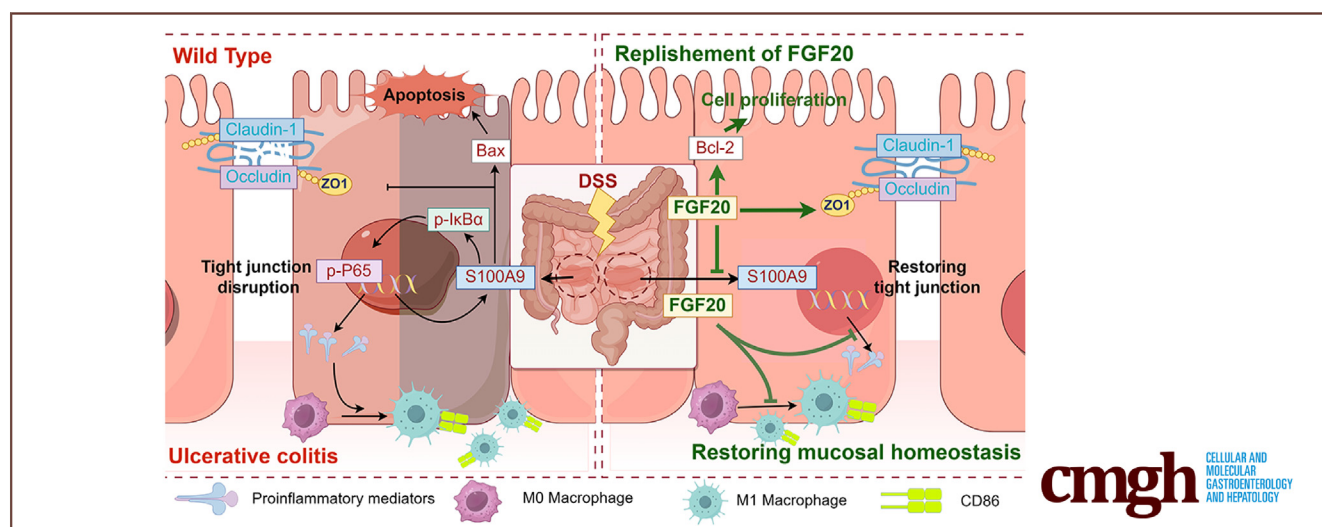# cmgh

ORIGINAL RESEARCH

Fibroblast Growth Factor 20 Attenuates Colitis by Restoring Impaired Intestinal Epithelial Barrier Integrity and Modulating Macrophage Polarization via S100A9 in an NF-κB-Dependent Manner

Dong Zhen,[1,*] Songxue Wang,[2,*] Zhen Liu,[2,*] Yiyuan Xi,[1,*] Hanlin Du,[1] Ningrui Wang,[2] Xiaotang Gao,[2] Zhuofeng Lin,[2,3] and Fan Wu[3]

[1]The First Affiliated Hospital of Wenzhou Medical University, Wenzhou, China; [2]School of Pharmaceutical Sciences, Wenzhou Medical University, Wenzhou, China; and [3]The Affiliated Songshan Lake Center Hospital, Guangdong Medical University, Dongguan, China

SUMMARY

Circulating and colonic fibroblast growth factor 20 (FGF20) levels were elevated in mice with colitis and the loss of FGF20 increasing susceptibility to colitis. The overexpression of FGF20 attenuates colitis by restoring impaired intestinal epithelial barrier integrity and modulating macrophage polarization via S100A9.

BACKGROUND & AIMS: Exogenous recombinant fibroblast growth factor 20 (FGF20) protein has been proved to treat ulcerative colitis; however, its mechanism of action remains unclear. This study aimed to explore the role and mechanism of action of FGF20 in ulcerative colitis.

METHODS: Data from patients with ulcerative colitis were analyzed using the Gene Expression Omnibus dataset. A murine colitis model was established by administering 2% dextran sodium sulfate. FGF20 knockout mice and Adenoassociated viruses (AAV)-FGF20-treated mice were used to elucidate the

specific mechanisms. Proteomic analysis was conducted to identify differentially expressed genes.

RESULTS: FGF20 levels were significantly elevated in the colonic tissues of subjects and mice with colitis. FGF20 deficiency exacerbated dextran sodium sulfate–induced colitis; in contrast, FGF20 replenishment alleviated colitis through 2 principal mechanisms: restoration of impaired intestinal epithelial barrier integrity, and inhibition of M1 macrophage polarization. Notably, S100A9 was identified as a pivotal downstream target of FGF20, which was further demonstrated by pharmacologic inhibition and overexpression experiments of S100A9 using paquinimod (a specific inhibitor of S100A9) and AAV-S100A9 in FGF20 knockout and AAV-FGF20 mice with colitis, respectively. Additionally, the nuclear factor-κB pathway was found to be involved in the process by which FGF20 regulates S100A9 to counteract colitis.

CONCLUSIONS: These results suggest that FGF20 acts as a negative regulator of S100A9 and nuclear factor-κB, thereby inhibiting M1 macrophage polarization and restoring intestinal

epithelial barrier integrity in mice with dextran sodium sulfate–induced colitis. FGF20 may serve as a potential therapeutic target for the treatment of ulcerative colitis. *(Cell Mol Gastroenterol Hepatol 2025;19:101486; https://doi.org/10.1016/j.jcmgh.2025.101486)*

Inflammatory bowel disease (IBD) is a chronic, relapsing inflammatory condition that primarily affects the gastrointestinal tract but can also involve nearly any organ system. Ulcerative colitis (UC), a common form of IBD, is estimated to affect 5 million people worldwide in 2023, with its incidence rising annually.[1] The hallmark features of UC include mucosal ulcers, rectal bleeding, diarrhea, and abdominal pain, often accompanied by defects in the epithelial barrier.[2] These defects can lead to structural and functional changes in the colon, considerably affecting a patient's quality of life. Despite the substantial expansion of therapeutic options for UC, including biologics and small molecules, real-world remission rates for patients remain unsatisfactory.[3]

Dysregulated immune response and impaired intestinal epithelial barrier integrity are key pathophysiological characteristics of UC.[4] Previous studies have shown that the innate immune system in the intestinal mucosa (comprising neutrophils, monocytes/macrophages, and intraepithelial lymphocytes) plays a critical, if not more important, role in the development and progression of intestinal inflammation compared with the adaptive immune system.[5] In mice with colitis, abundant inflammatory cells are found in the lamina propria of the colonic mucosa, leading to chronic immune system activation and persistent gastrointestinal inflammation.[6] Similarly, colonic specimens from patients with UC show an accumulation of macrophages, which are involved in the initiation and resolution of inflammation.[7] Classically activated M1 macrophages are associated with the onset and persistence of inflammation, whereas M2 or M2-like macrophages are linked to the resolution of chronic inflammation.[8] Abnormal polarization of macrophages in intestinal tissues has been observed in patients with IBD,[9] and as such, macrophages are considered potential therapeutic targets for UC, because they play a key role in inflammation resolution and tissue repair.

Fibroblast growth factor 20 (FGF20), first isolated from *Xenopus laevis*, is a member of the paracrine FGF9 subfamily. It is expressed primarily in the brain (The Human Protein Atlas, www.proteinatlas.org) and has a wide range of biologic functions, including roles in embryonic development, cell growth, organ development, tissue repair, and tumor progression.[10–13] FGF20 (CG53135) has been shown to reduce the severity of oral mucositis induced by radiation or chemotherapy/radiation,[14] leading to its approval by the Food and Drug Administration for clinical trials targeting oral mucositis in patients with cancer. However, this clinical trial was terminated in phase II because of unclear therapeutic targets.[15] Additionally, recombinant human FGF20 has shown promise in treating traumatic brain injury by upregulating junction protein expression, inhibiting inflammation, and promoting vascular repair and angiogenesis.[16,17] Notably, FGF20 has demonstrated therapeutic efficacy in experimental models of intestinal inflammation.[18] However, the exact regulatory mechanisms through which FGF20 exerts its effects in the treatment of UC remains unclear. Investigating these mechanisms is crucial for establishing FGF20 as a potential therapeutic candidate for human IBD.

S100A9, a member of the S100 protein family, is a calcium sensor found in neutrophils and monocytes/macrophages.[19] S100A9 is recognized as a sensitive biomarker for monitoring disease activity in IBD and other inflammation-related disorders.[20] Previous studies have indicated that S100A9 can induce nuclear factor kappa B (NF-κB) activity, and targeting NF-κB in colon cancer cells may promote M1-like macrophage polarization.[21] In this study, we explored whether FGF20 protects against colitis-induced colonic damage and impaired intestinal epithelial barrier integrity by regulating S100A9. Our results show that FGF20 levels were elevated in mice with colitis. Dextran sulfate sodium (DSS)-induced colitis was more severe in FGF20 knockout (KO) mice and alleviated by replenishing FGF20. We further found that FGF20 protects against colitis by restoring intestinal epithelial barrier integrity and modulating macrophage polarization through S100A9 in an NF-κB-dependent manner.

Results

FGF20 is Markedly Increased in Patients and Mice with Colitis

To investigate changes in FGF20 expression, an expression dataset from patients with UC was downloaded from National Center for Biotechnology Information's Gene Expression Omnibus (GSE22619) and analyzed. Analyses of public datasets indicated that FGF20 mRNA levels were significantly elevated in UC specimens compared with healthy control subjects (Figure 1A). To validate these findings, a mouse model of UC was established using DSS treatment. DSS-induced mice displayed typical colitis symptoms, including shaggy hair, weight loss, diarrhea, and occult fecal blood, which closely resembled colitis symptoms in humans. Specifically, DSS-treated mice exhibited

considerable body weight loss and elevated disease activity index (DAI) scores compared with control animals (Figure 1B and C), along with shortened colon length (a key marker of colorectal inflammation severity) (Figure 1D).

Histopathologic analysis further revealed severe alterations in the colonic tissues of DSS-treated mice, including epithelial damage and crypt loss (Figure 1E). Immunoblotting and immunohistochemistry analyses demonstrated markedly increased FGF20 expression in the colonic tissue of DSS-treated mice (Figure 1F and G), and serum FGF20 levels were also elevated (Figure 1H). Additionally, FGFR4, but not FGFR1, FGFR2, or FGFR3, was upregulated following DSS treatment (Figure 1I), suggesting that FGFR4 may be the primary receptor through which FGF20 acts in this context. These findings suggest that FGF20 plays a major role in the pathogenesis of colitis.

FGF20 Deficiency Exacerbates DSS-Induced Colitis in Mice

Building on the observation of increased FGF20 in colitis, we investigated its functional significance by generating FGF20 KO mice. These mice were created by replacing most of exon 1 and all of exons 2 and 3 of the FGF20 gene with the IRES-LacZ-polyA/PGK-neo cassette, and their genotype was confirmed through polymerase chain reaction (PCR) and immunoblot analysis (Figure 2A and B). After DSS administration, FGF20 KO mice exhibited greater weight loss, higher DAI scores, and shorter colon lengths compared with wild-type (WT) control animals (Figure 3A-C). Histopathologic analysis further revealed that FGF20 KO mice displayed severe disruption of the colonic mucosal structure and a marked reduction in goblet cell numbers, as demonstrated by hematoxylin-eosin and periodic acid–Schiff (PAS) staining, respectively (Figure 3D). Additionally, the expression levels of proinflammatory mediators, such as inducible nitric oxide synthase (iNOS) and interleukin (IL)6, which are known to drive colitis progression, were significantly higher in FGF20 KO mice with colitis than in WT control animals (Figure 3E). These findings indicate that FGF20 deficiency exacerbates DSS-induced inflammation and compromises intestinal tissue integrity, underscoring its protective role in colitis.

FGF20 Overexpression Attenuates DSS-Induced Colitis in Mice

To further investigate the role of FGF20 in colitis development, WT mice were treated with adenoassociated virus (AAV) expressing FGF20 (AAV-FGF20). As expected, AAV-FGF20 treatment significantly increased FGF20 expression levels (Figure 2C) and mitigated DSS-induced colitis, showing the opposite phenotype compared with FGF20 KO mice. Specifically, AAV-FGF20 mice exhibited less weight loss, lower DAI scores, and reduced colon shortening compared with WT mice after 5 days of DSS treatment (Figure 4A-C). Histologic analyses revealed that DSS-induced disruption of the colonic mucosal structure and loss of goblet cells were alleviated in AAV-FGF20-treated mice (Figure 4D). Additionally, AAV-FGF20 treatment

prominently reduced the expression levels of proinflammatory mediators, including iNOS and IL6, compared with control subjects (Figure 4E). Collectively, these findings demonstrate a protective role of FGF20 in the progression of DSS-induced colitis.

FGF20 Improves the Impaired Intestinal Epithelial Barrier Integrity in DSS-Induced Colitis Mice

Intestinal epithelial barrier integrity is essential for maintaining intestinal homeostasis; in contrast, its dysfunction increases intestinal permeability and exacerbates the inflammatory response in colitis.[22] To assess whether FGF20 influences intestinal permeability in DSS-induced colitis, the concentration of fluorescein isothiocyanate-labeled dextran (FITC-dextran 4000) in plasma was measured. As shown in Figure 5A, plasma FITC-dextran 4000 levels were significantly elevated in WT mice after DSS treatment and further increased in FGF20 KO mice, indicating that FGF20 deficiency exacerbates intestinal permeability under pathologic conditions.

The intestinal epithelial barrier comprises epithelial cells and intercellular tight junctions, with such proteins as ZO-2, occludin, and claudin-1 being critical components.[23] To clarify FGF20's role in intestinal barrier integrity during DSS-induced colitis, the expression of ZO-2, occludin, and claudin-1 was analyzed by immunoblotting. The proteins were markedly downregulated in DSS-treated WT mice, with an even greater reduction observed in DSS-treated FGF20 KO mice (Figure 5B). Consistently, immunofluorescence analysis revealed red fluorescence for occludin and claudin-1 in DSS-induced FGF20 KO mice compared with DSS-induced WT mice (Figure 6A and B). Continuous proliferation of intestinal epithelial cells is crucial for maintaining the self-renewal and integrity of the intestinal barrier.[24] Immunofluorescence staining for the proliferation marker Ki67 showed a marked reduction in Ki67-positive cells in mice with colitis compared with littermate control animals, with further decreases in FGF20 KO mice (Figure 5C). Immunoblot analysis of Bcl-2-associated X protein (Bax) and Bcl-2 also demonstrated FGF20's positive impact on colonic tissue proliferation. FGF20 deficiency worsened the DSS-induced decrease in Bcl-2 and the increase in Bax levels (Figure 5D). Conversely, treatment with exogenous FGF20 significantly mitigated the DSS-induced downregulation of colonic ZO-2, occludin, claudin-1, Ki67-positive cells, and Bcl-2, and the upregulation of colonic Bax (Figure 7A-C, Figure 6C and D). These findings suggest that FGF20 plays a protective role in maintaining the integrity of the intestinal epithelial barrier in mice with colitis.

FGF20 Restrain M1-like Macrophage Polarization in DSS-Induced Colitis Mice

In response to ulcerative damage during colitis, cytokine gene expression is altered, accompanied by considerable immune cell infiltration.[25] To assess whether immune cell infiltration changes after DSS treatment, we compared the infiltration of Mϕs (F4/80), neutrophils (Ly6G), B cells
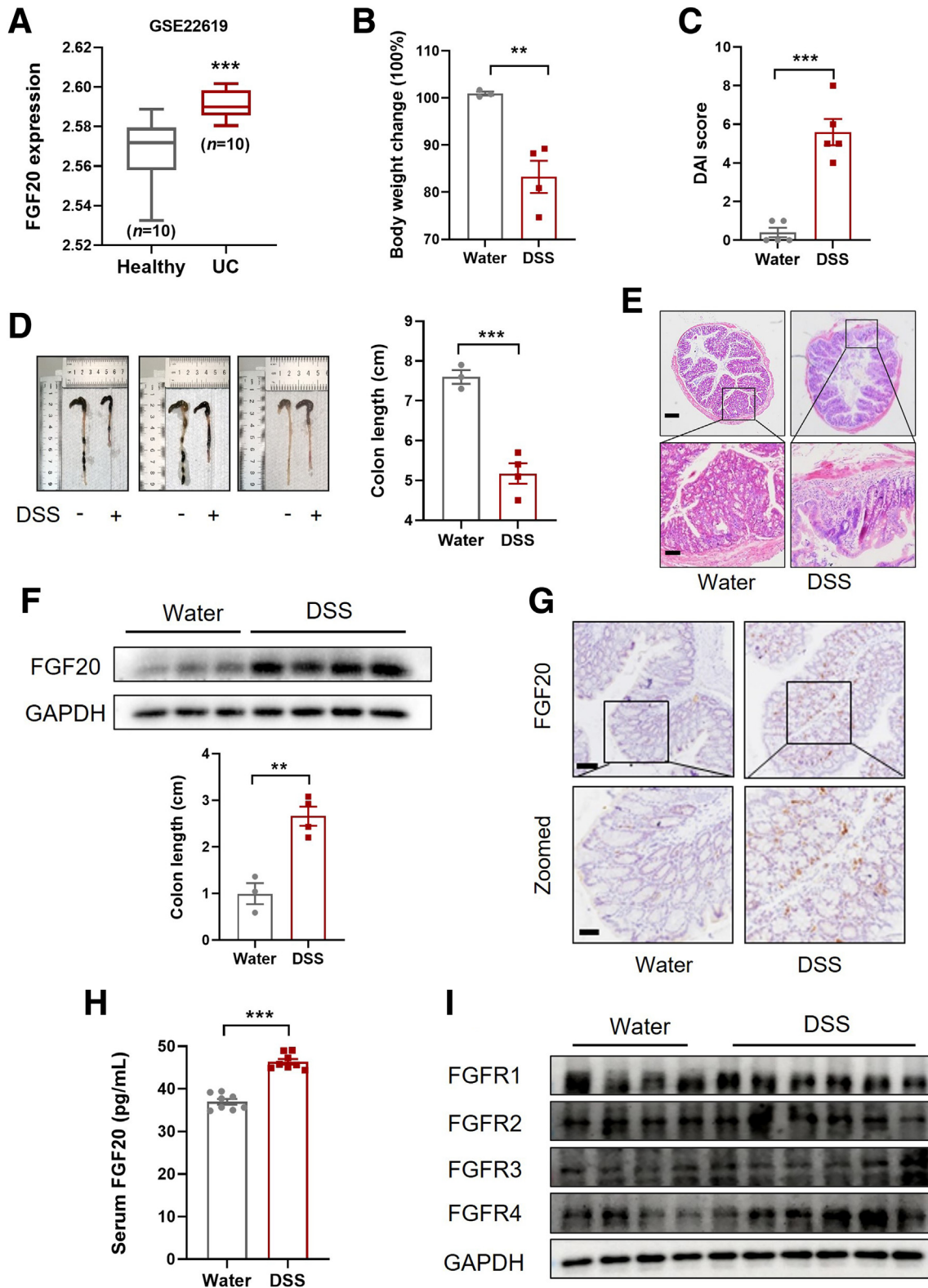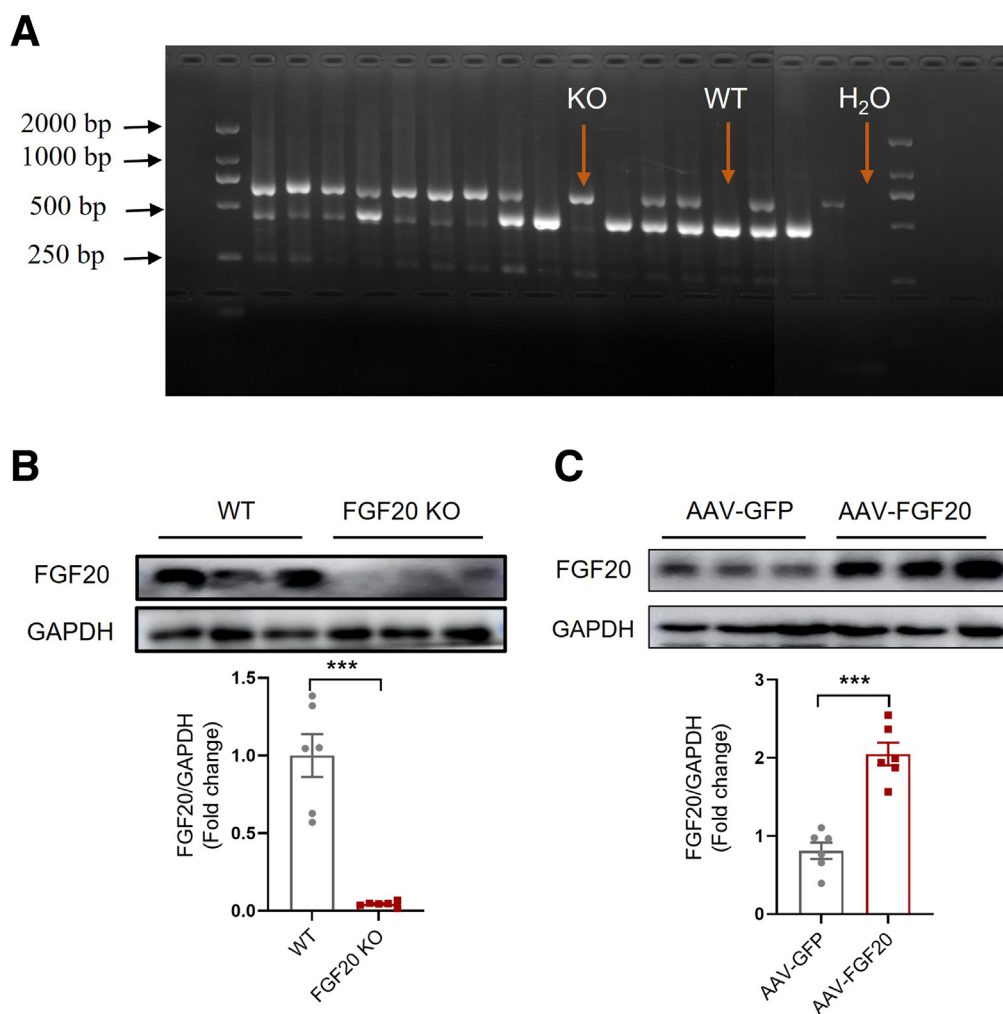
Figure 1. FGF20 is markedly increased in patients and mice with colitis. (*A*) Box plot of FGF20 mRNA in healthy control animals and ulcerative colitis specimens (using dataset GSE22619). (*B-D*) The body weight, DAI scores, and gross morphology images of colons and colon lengths of each group were recorded (n ≥ 3). (*E*) hematoxylin and eosin (H&E)-stained colonic sections of each group mice. Scale bar, 100 μm and 50 μm (n ≥ 3). (*F, G*) Expression of FGF20 in the colon of each group of mice was detected by Western blot and immunohistochemistry (n ≥ 3). Scale bar, 50 μm and 20 μm. (*H*) Serum FGF20 contents were measured by enzyme-linked immunosorbent assay (n = 8). (*I*) Expression of FGFR1, FGFR2, FGFR3, and FGFR4 were detected by Western blot (n ≥ 3). Data are represented as mean ± standard error of the mean (SEM); *$P < .05$, **$P < .01$, ***$P < .001$.

A

B

C

Figure 2. Genotyping of FGF20 KO null mice and AAV-FGF20. (A) Results of the identification of various genotypes. Homozygotes: 1 band with 639 bp. Heterozygotes: 2 bands with 639 bp and 473 bp. Wild-type allele: 1 band with 473 bp. (B, C) The expression of FGF20 in FGF20 KO mice and AAV9-FGF20 overexpression mice were measured by Western blot (n = 6). Data are represented as mean ± SEM; ***$P < .001$.

(CD45), and CD4$^+$ T cells (CD4) in the colonic tissues of WT and FGF20 KO mice. Although there was no difference in the infiltration of CD4$^+$ T cells, B cells, or neutrophils between FGF20 KO and WT mice after DSS treatment, a marked increase in macrophage infiltration was observed in the colonic tissues of FGF20 KO mice (Figure 8).

Prior studies have shown that macrophages are abundant in colon specimens from patients with UC,[26] and modulation of macrophage polarization can influence the severity of DSS-induced colitis.[27] Given that FGF20 affects macrophage infiltration, we next examined whether the loss or overexpression of FGF20 impacts macrophage polarization. We validated changes in mRNA expression related to M1 and M2 macrophage polarization in the colonic tissue using quantitative PCR. As expected, M1 polarization-related genes, including *IL-6*, *TNF-α*, *IL-1β*, and *MCP-1*, were significantly upregulated in the colonic tissue of WT mice after DSS administration. This upregulation was further exacerbated in FGF20 KO mice but ameliorated in AAV-FGF20-treated mice (Figure 9A and C). These trends in M1 polarization were consistent across all colitis models. In contrast, M2 polarization-related genes, including *IL-10*, *Arg-1*, and *Ym1*, were significantly upregulated by DSS

treatment in WT mice; in contrast, they were inhibited in FGF20 KO mice and further upregulated in AAV-FGF20 mice (Figure 9B and D). However, *Fizz1* exhibited the opposite trend compared with other M2-related genes (Figure 9B and D). Collectively, these data suggest that FGF20 alleviates DSS-induced colitis by reducing macrophage infiltration and restraining M1-like macrophage polarization.

FGF20 Deficiency Increases Colonic S100A9 Expression in DSS-Induced Colitis Mice

To explore the underlying mechanisms of FGF20's protective role in colitis, we conducted a Data-independent Acquisition-based proteomic analysis. In the DSS-induced colitis model, a total of 119 differently expressed proteins were identified, including 84 upregulated and 35 down-regulated proteins (defined by fold change ≤0.67 or fold change ≥1.5 and $P < .05$) (Figure 10A). Notably, S100A9, a calcium-binding protein widely recognized as a biomarker of inflammation,[28,29] was found among the upregulated proteins (Figure 10B). Proteomic analysis revealed that the DSS-induced increase in S100A9 in WT mice was further amplified in FGF20 KO mice (Figure 10C). This finding was
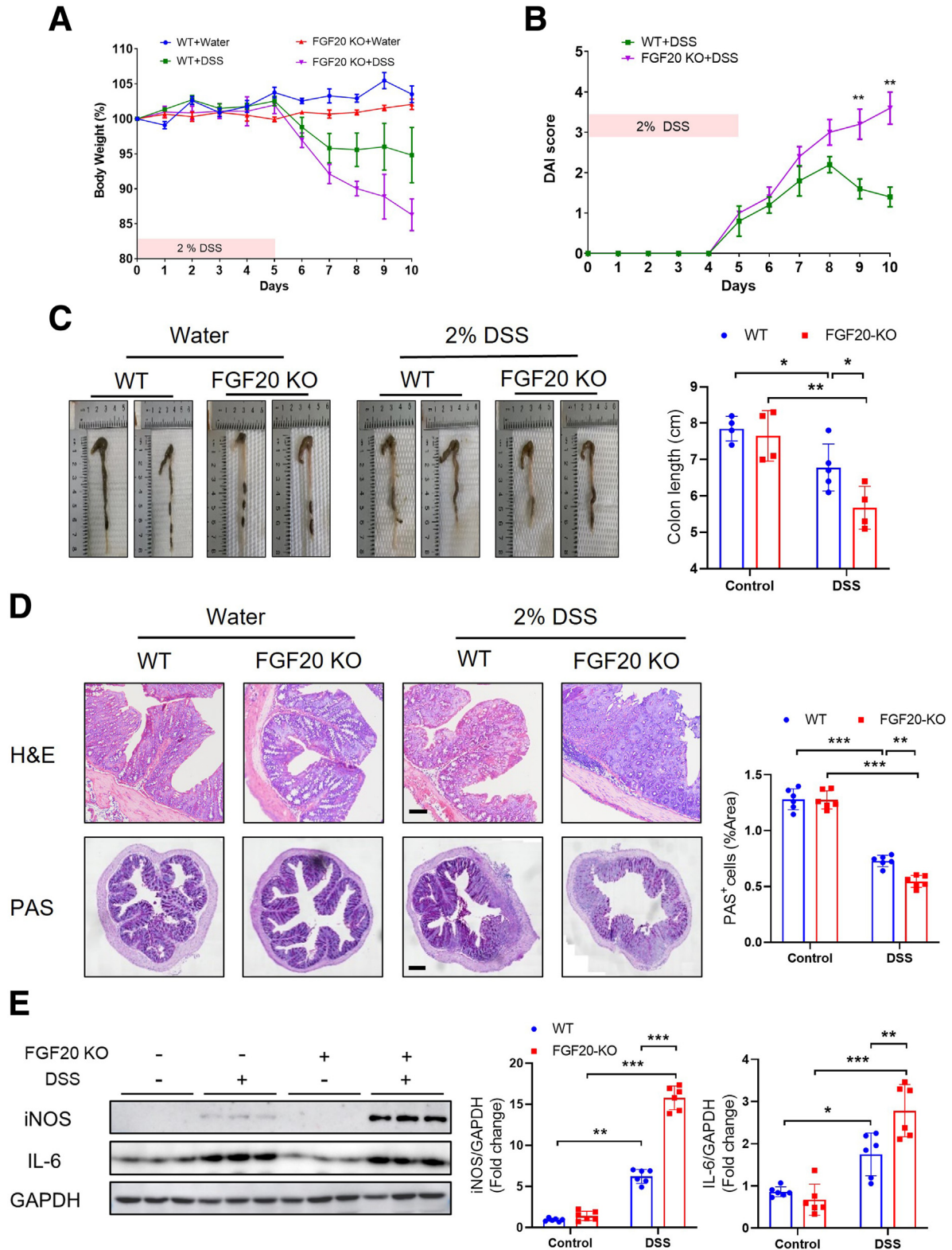
Figure 3. FGF20 deficiency exacerbates the development of DSS-induced colitis. Eight-week-old male FGF20 KO mice and WT littermates were given 2% DSS in drinking water for 5 days, followed by normal drinking water for an additional 5 days. (*A-C*) Body weights, DAI, and gross morphology images of colons and colon lengths in FGF20 KO and WT mice with or without colitis were recorded (n ≥ 4). (*D*) H&E (*top*) and PAS (*bottom*) stained colonic sections of each group mice. Scale bar, 100 μm and 50 μm. (*E*) Immunoblot analysis of colonic IL6 and iNOS contents in FGF20 KO and WT mice with or without colitis (n = 6). Data are represented as mean ± SEM; *P < .05, **P < .01, ***P < .001.
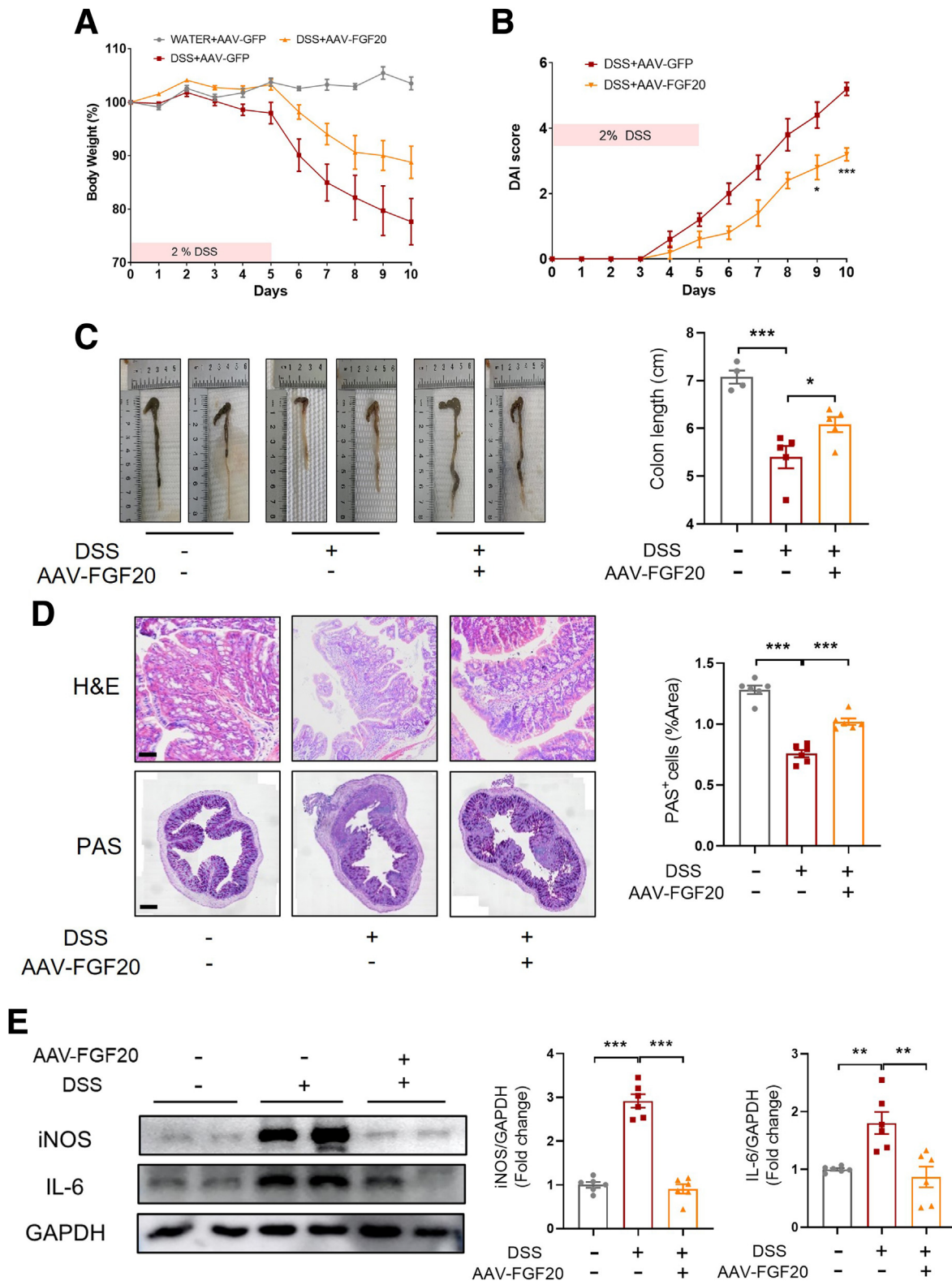
Figure 4. FGF20 overexpression attenuates DSS-induced colitis. Six-week-old male WT mice were treated with AAV-FGF20 or AAV-GFP by tail vein injection. After 4 weeks of AAV injection, all mice were given 2% DSS in drinking water for 5 days, followed by normal drinking water for an additional 5 days. (*A-C*) Body weights, DAI scores, and gross morphology images of colons and colon lengths in AAV-FGF20- or AAV-GFP-treated mice with or without colitis were recorded (n ≥4). (*D*) H&E (*top*) and PAS (*bottom*) stained colonic sections of each group mice. Scale bar, 20 μm and 50 μm. (*E*) Immunoblot analysis of colonic iNOS and IL6 contents in AAV-FGF20- or AAV-GFP-treated mice with or without colitis (n = 6). Data are represented as mean ± SEM; *P < .05, **P < .01, ***P < .001.
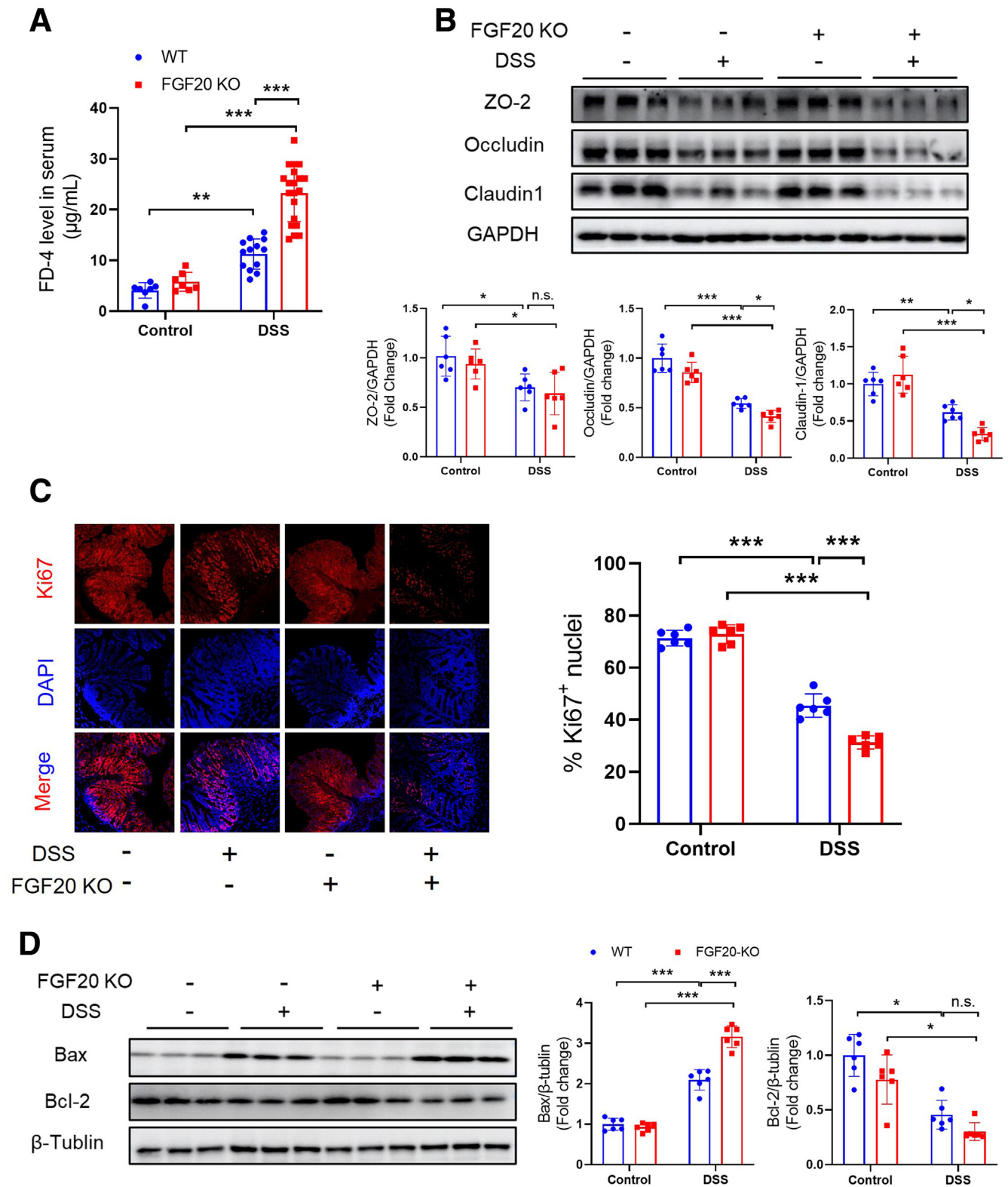
Figure 5. FGF20 deficiency aggravates impaired intestinal epithelial barrier integrity in DSS-induced colitis mice. (*A*) The contents of plasma FITC-dextran 4000 level were measured (n = 7). (*B*) Western blot and quantitation of colonic ZO-2, occludin, and claudin-1 expression in FGF20 KO and WT control with or without colitis (n = 6). (*C*) Representative fluorescence images of Ki67, and the percentage of Ki67-positive cells in FGF20 KO mice and WT littermates with or without colitis (n ≥ 7). Scale bar, 50 μm. (*D*) Immunoblot analysis of colonic Bax and Bcl-2 expression in FGF20 KO mice and WT mice with colitis or not (n = 6). Data are represented as mean ± SEM; *P < .05, **P < .01, ***P < .001. n.s., no significance.
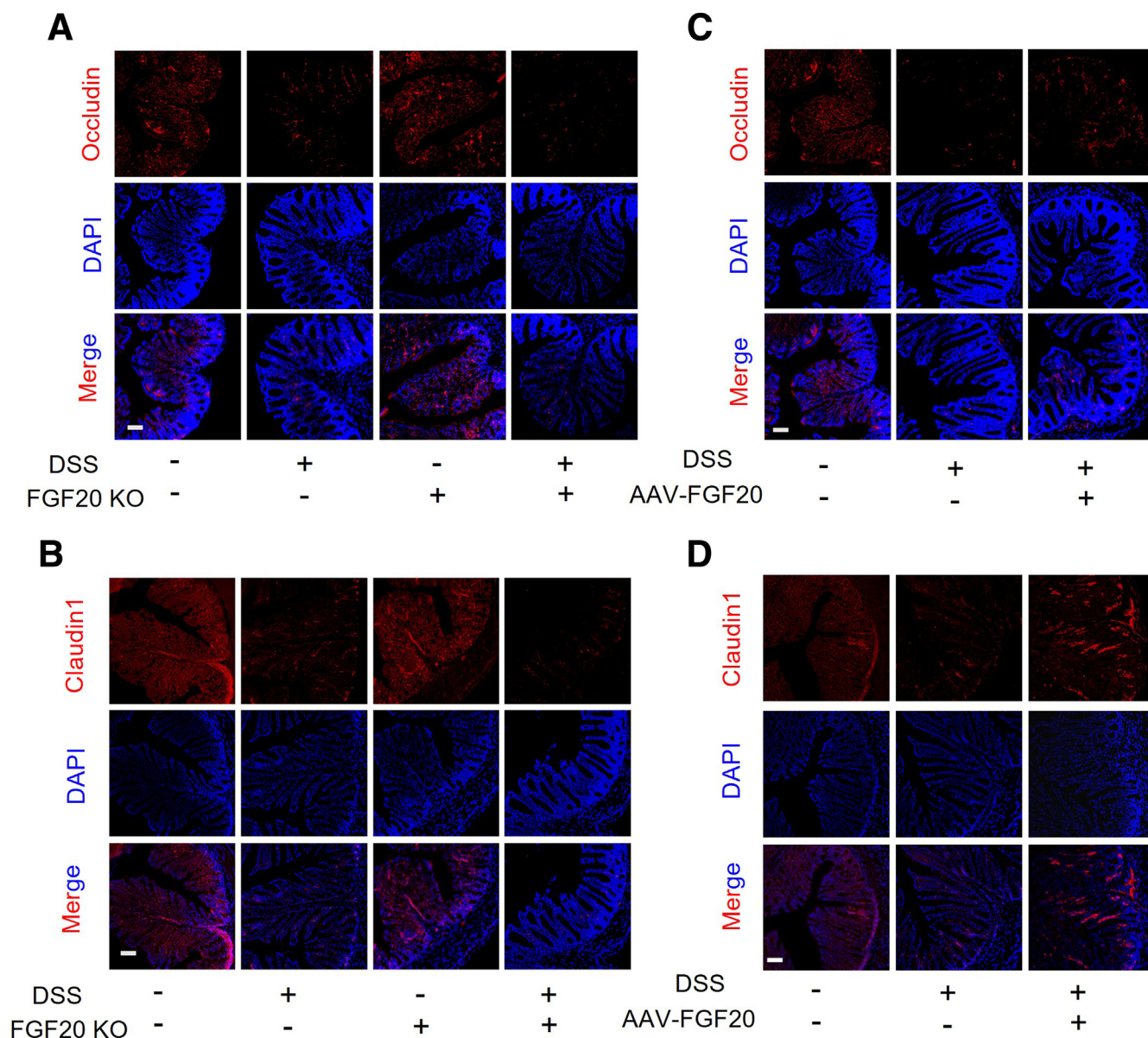
Figure 6. FGF20 regulates occludin in DSS-induced colitis mice. Representative fluorescence images of colonic occludin (*A, C*) and claudin-1 (*B, D*) from FGF20 KO and WT control mice with or without colitis, and AAV-FGF20- and AAV-GFP-treated mice with or without colitis. Scale bar, 50 μm.

corroborated by immunoblot analysis, which showed markedly elevated colonic S100A9 protein levels in WT mice with colitis compared with their WT littermates (Figure 10*D*). Importantly, S100A9 expression was even higher in the colons of FGF20 KO mice with colitis (Figure 10*D*). Similar results were confirmed by immunohistochemistry (Figure 10*E*). These findings suggest that S100A9 may be a downstream target of FGF20, mediating its protective effects against DSS-induced colitis in mice.

Pharmaceutic Inhibition of S100A9 Protects Against DSS-Induced Colitis in FGF20 KO Mice

To determine whether S100A9 is critical for FGF20's regulation in colitis, paquinimod, a specific S100A9 inhibitor, was administered intraperitoneally (10 mg/kg/day) to both WT and FGF20 KO mice with or without colitis to block S100A9 activity. Inhibition of S100A9 significantly reversed the exacerbated weight loss and shortened colon length seen in FGF20 KO mice (Figure 11*A* and *B*). Histologic analysis with hematoxylin-eosin and PAS staining confirmed the protective effects of paquinimod, showing reduced injury to the colonic mucosal structure and less loss of goblet cells in paquinimod-treated FGF20 KO mice compared with untreated FGF20 KO control animals (Figure 11*C*). Additionally, the elevated colonic expression of iNOS and IL6 induced by FGF20 deficiency was attenuated by paquinimod treatment in FGF20 KO mice with colitis (Figure 11*D*). These results indicate that inhibition of
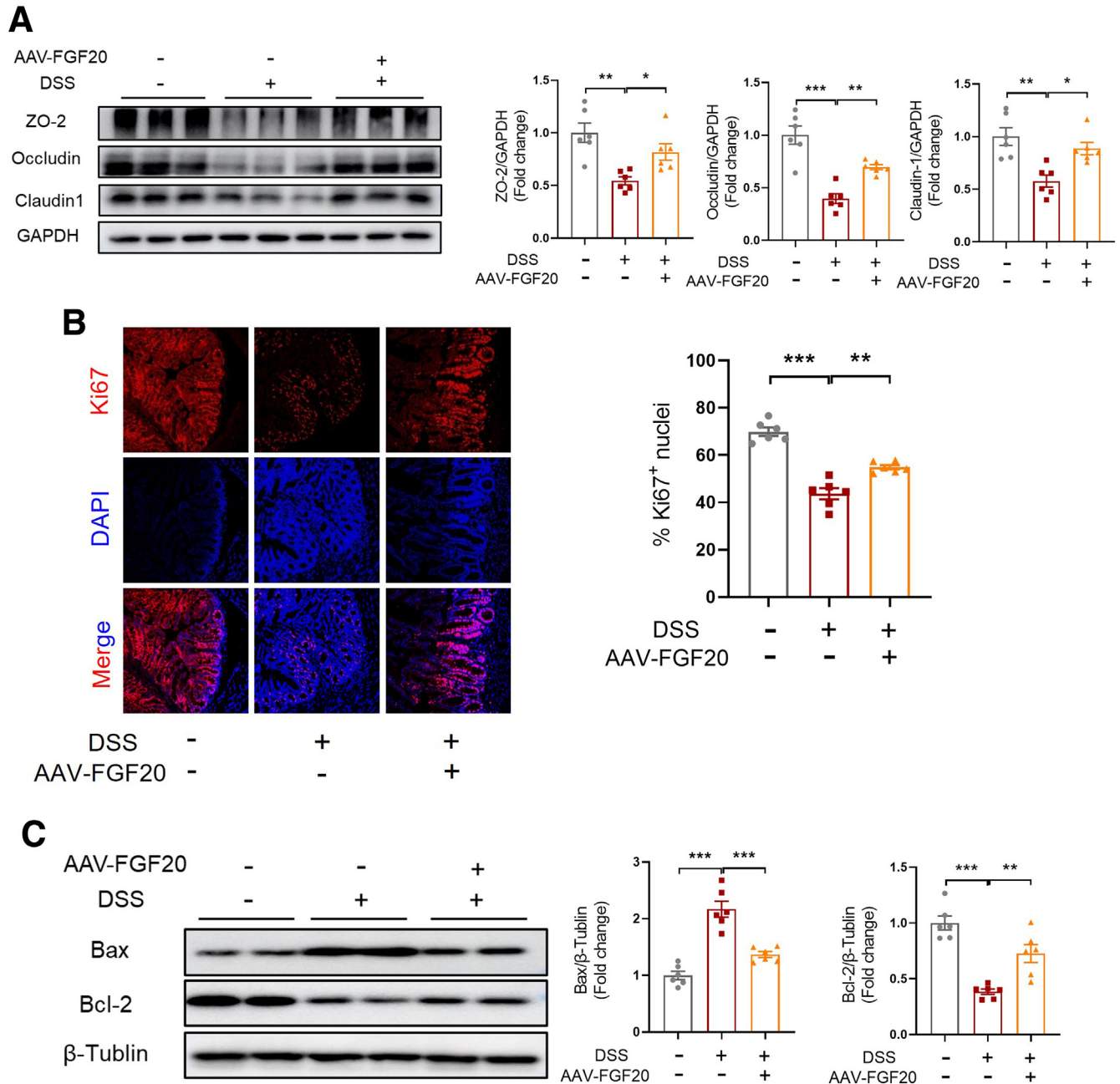
Figure 7. FGF20 overexpression improves the impaired intestinal barrier integrity in DSS-induced colitis mice. (*A*) Western blot and quantitation of colonic ZO-2, occludin, and claudin-1 expression in AAV-FGF20- and AAV-GFP-treated mice with or without colitis (n = 6). (*B*) Representative fluorescence images of Ki67, and the percentage of Ki67-positive cells in AAV-FGF20- and AAV-GFP-treated mice with or without colitis (n ≥ 5). Scale bar, 50 μm. (*C*) Immunoblot analysis of colonic Bax and Bcl-2 expression in AAV-FGF20- and AAV-GFP-treated mice with or without colitis (n = 6). Data are represented as mean ± SEM; *P < .05, **P < .01, ***P < .001.

S100A9 is a key downstream target of FGF20 in the progression of DSS-induced colitis.

Overexpression of S100A9 Attenuates the Protective Effects of AAV-FGF20 Against DSS-Induced Mice Colitis

To further explore the role of S100A9 in FGF20-mediated protection against DSS-induced colitis, AAV-FGF20 mice were treated with AAV9 vectors carrying S100A9 (AAV-S100A9) or AAV-GFP with the cTNT core promoter via tail vein injection. An obvious increase in colonic S100A9 expression was observed in the AAV-S100A9-treated mice (Figure 12*A*). Notably, overexpression of S100A9 significantly diminished the protective effects of AAV-FGF20 in DSS-induced colitis, as evidenced by exacerbated weight loss and shortened colon length (Figure 12*B* and *C*). Histologic
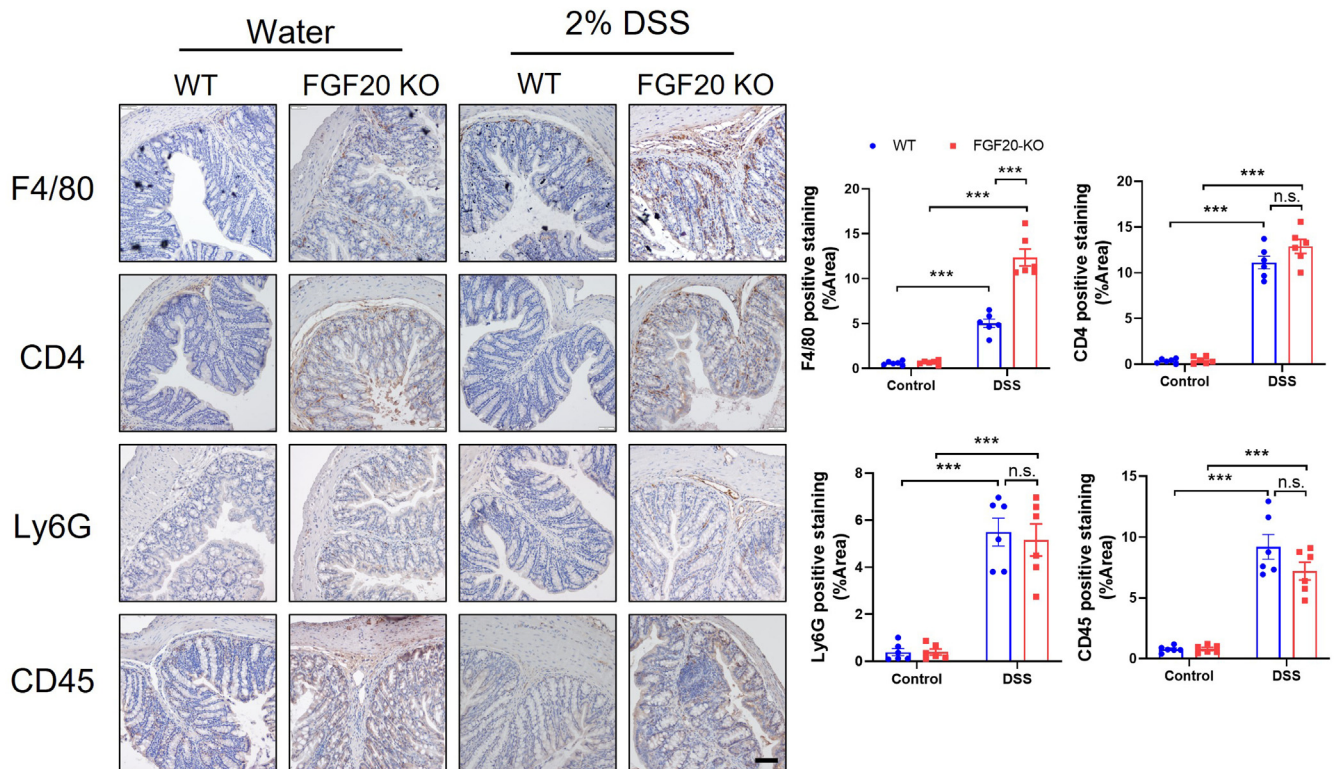
Figure 8. Increased infiltration of macrophage in the colonic tissues of FGF20 KO mice and WT mice treated with DSS or not. Representative immunohistochemistry images of colonic sections from WT and FGF20 KO mice and stained with F4/80, CD4, Ly6G, and B220 (n ≥ 6). Scale bar, 50 μm. Data are represented as mean ± SEM; ***$P <$ .001 n.s., no significance.

analysis revealed thickening of the colon wall, shortening of intestinal villi, and loss of goblet cells in AAV-FGF20 mice treated with AAV-S100A9 compared with AAV-FGF20 control animals (Figure 12D). Furthermore, treatment with AAV-S100A9 partially reversed the inhibitory effects of AAV-FGF20 on the elevated expression of iNOS and IL6 in mice with colitis (Figure 12E). These results suggest that S100A9 acts as a negative regulator, modulating the protective effects of FGF20 against DSS-induced colitis.

S100A9 Negatively Affects FGF20 Mediated Restoration of Impaired Intestinal Epithelial Barrier Integrity

Our data indicated that FGF20 could restore intestinal epithelial barrier integrity and that S100A9 might be a crucial downstream regulator of FGF20. Therefore, we investigated whether S100A9 influences the ameliorative effects of FGF20 on intestinal epithelial barrier function. Consistent with the previously mentioned results, inhibition of S100A9 by paquinimod significantly reversed the decrease in ZO-2, occludin, and claudin-1 in DSS-induced FGF20 KO mice (Figure 13A). This finding was further confirmed by immunofluorescence analysis, which showed increased red fluorescence (Figure 14A). Regarding intestinal epithelial cell proliferation, paquinimod treatment also increased the number of Ki67-positive cells (Figure 13B), upregulated Bcl-2 expression, and downregulated Bax

expression in FGF20 KO mice with colitis, compared with FGF20 KO mice without treatment (Figure 13C). These results suggest that inhibition of S100A9 could reverse the adverse effects of FGF20 deficiency on intestinal epithelial barrier integrity.

On the other side, we also assessed the effect of S100A9 overexpression on the ameliorative effects of AAV-FGF20 on intestinal epithelial barrier integrity in mice with colitis. Not surprisingly, overexpression of S100A9 eliminated the beneficial effects of AAV-FGF20 on the DSS-induced downregulation of ZO-2, occludin, and claudin-1 (Figures 15A and 14B). Additionally, administration of AAV-S100A9 markedly diminished the proproliferative effects of AAV-FGF20 on intestinal epithelial cells, as evidenced by a decrease in Ki67-positive cells (Figure 15B), elevated Bax levels, and reduced Bcl-2 levels (Figure 15C). These data indicate that the positive effect of AAV-FGF20 on intestinal epithelial barrier restoration can be attenuated by overexpression of S100A9. Collectively, these results suggest that S100A9 negatively affects FGF20-mediated restoration of intestinal epithelial barrier function.

The Inhibition of FGF20 on M1-Like Macrophage Polarization in DSS-Induced Colitis is S100A9-Dependent

Our previous data showed that FGF20 inhibits M1-like macrophage polarization and negatively regulates S100A9
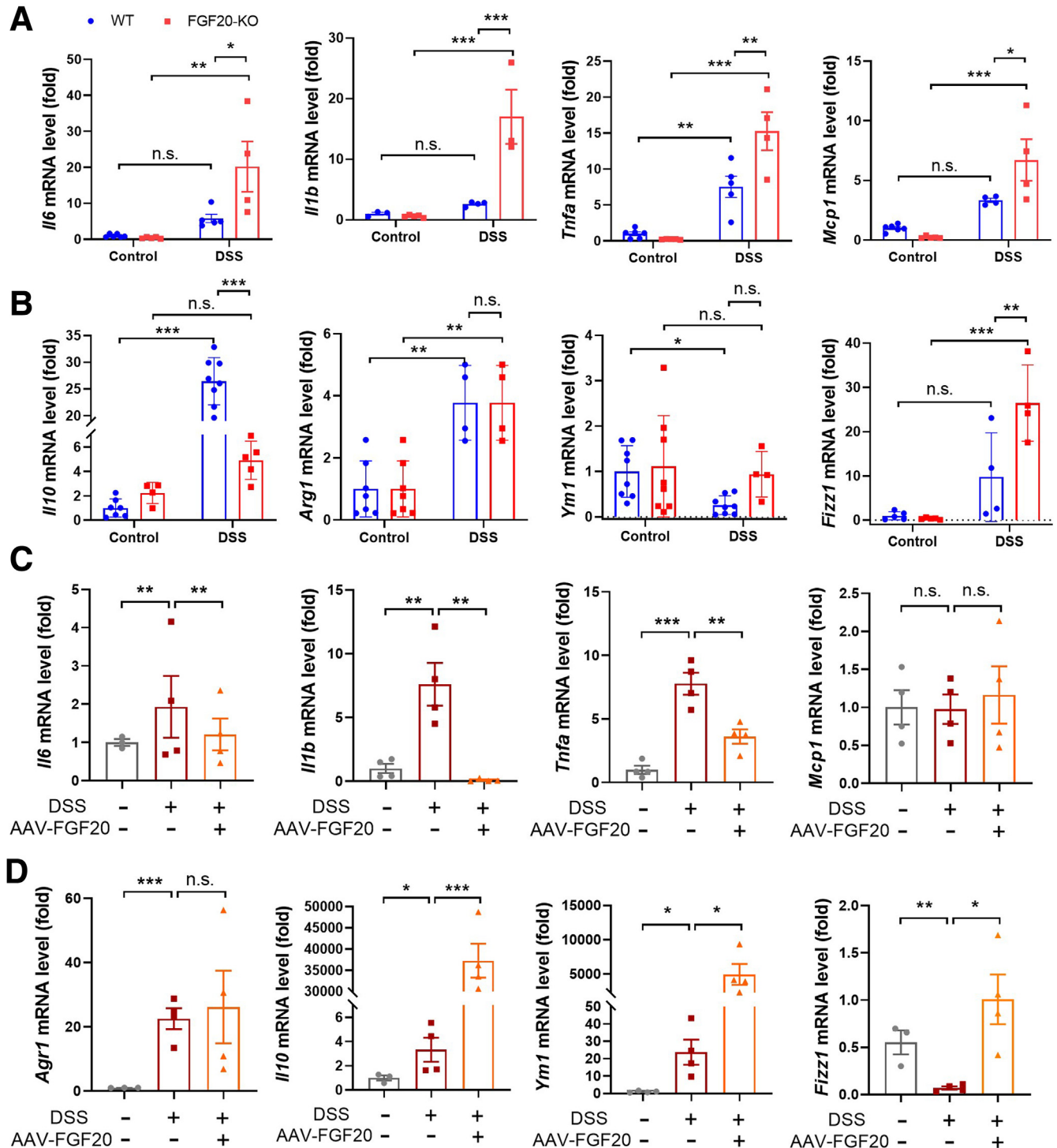
Figure 9. FGF20 restrain M1-like macrophage polarization in DSS-induced colitis mice. (*A, B*) mRNA expression levels of macrophage M1 (*IL-6, TNF-α, IL-1β*, and *MCP-1*) and M2 (*IL-10, Arg-1, Fizz1*, and *Ym1*) polarization-related gene in FGF20 KO and WT control with or without colitis were quantitatively determined by quantitative PCR (n ≥ 4). (*C, D*) mRNA expression levels of macrophage M1 (*IL-6, TNF-α, IL-1β*, and *MCP-1*) and M2 (*IL-10, Arg-1, Fizz1*, and *Ym1*) polarization-related gene in AAV-FGF20- and AAV-GFP-treated mice with or without colitis were quantitatively determined by quantitative PCR (n ≥ 4). Data are represented as mean ± SEM; *$P < .05$, **$P < .01$, ***$P < .001$. n.s., no significance.

expression in DSS-induced colitis. Thus, we investigated whether FGF20 inhibits M1-like macrophage polarization through its effect on S100A9. As expected, the increased

mRNA levels of M1 polarization-related genes (IL6, tumor necrosis factor [TNF]-α, IL1β, and MCP-1) in FGF20 KO mice with colitis were reversed by the administration of
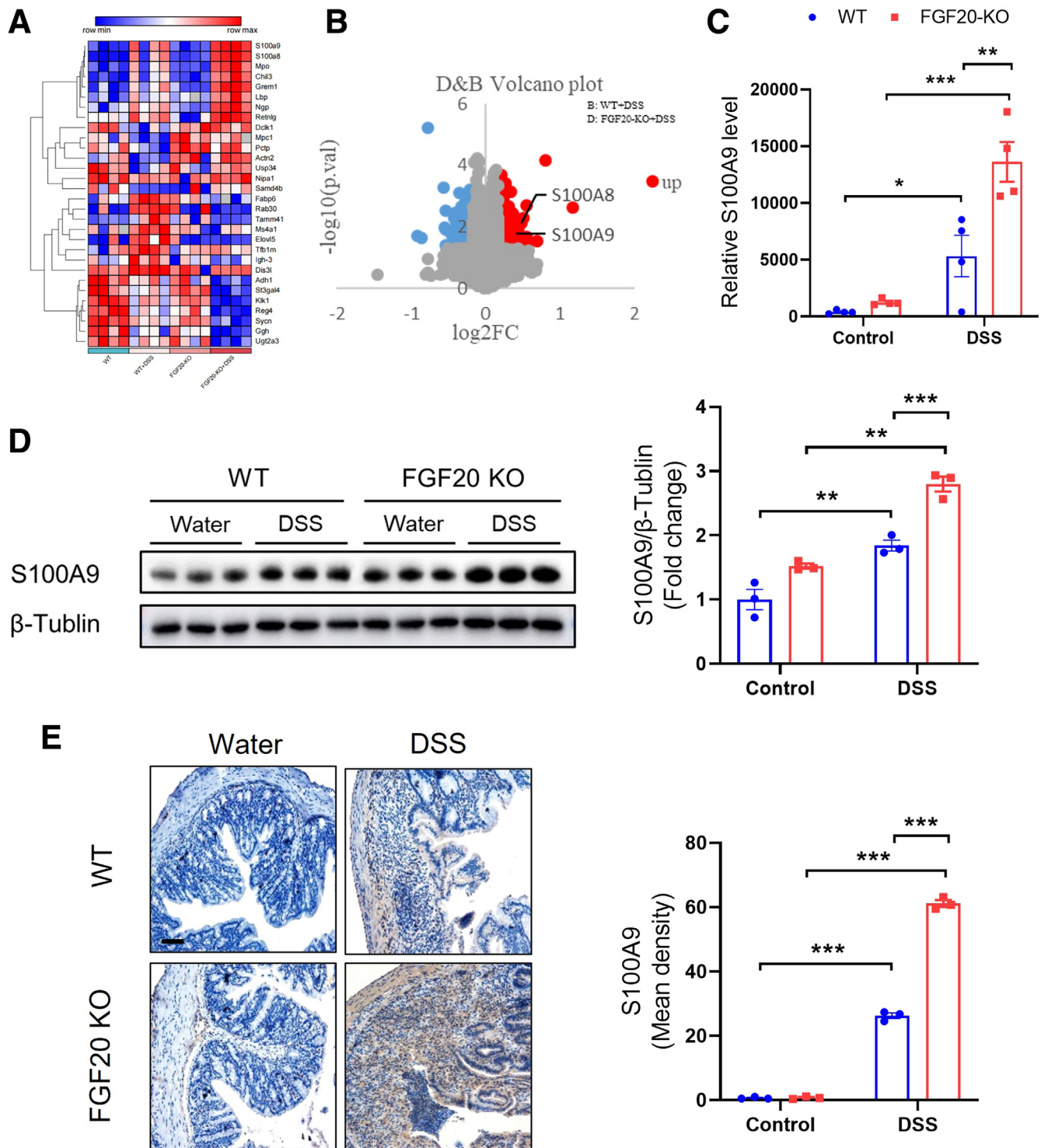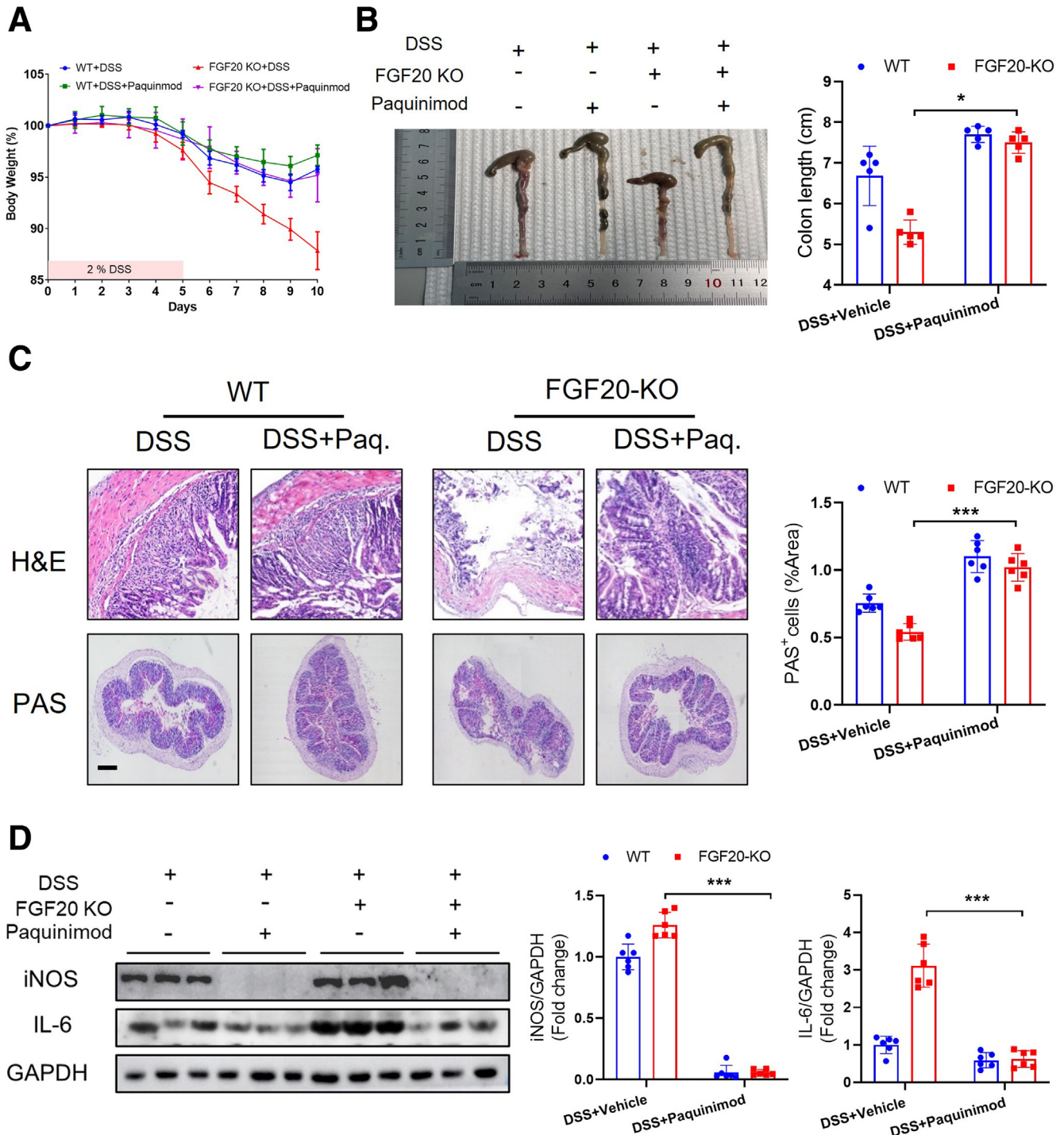
Figure 10. The loss of FGF20 increases colonic S100A9 expression in DSS-induced mice. (A) Heat maps of differentially expressed proteins in the colonic tissue of FGF20 KO and WT mice with or without colitis. (B) Volcano diagram of proteomic analysis in FGF20 KO and WT mice with colitis. (C) Relative expression data of S100A9 in FGF20 KO and WT mice with or without colitis (n = 4). (D, E) The expression of S100A9 in the colonic tissue of each group of mice was tested by Western blot (n = 3) and immunohistochemistry (n = 4). Data are represented as mean ± SEM. Scale bar, 50 μm. *P < .05, **P < .01, ***P < .001.

paquinimod (Figure 16A). Furthermore, overexpression of S100A9 in AAV-FGF20-treated mice with colitis partially counteracted the inhibitory effects of AAV-FGF20 on M1-like

macrophage polarization (Figure 16C). However, both S100A9 inhibition and overexpression in FGF20 KO mice with colitis and AAV-FGF20-treated mice with colitis

Figure 11. Inhibition of S100A9 protects against colitis in FGF20 KO mice. Eight-week-old male FGF20 KO mice and WT littermates were given 2% DSS in drinking water for 5 days, followed by normal drinking water for an additional 5 days. In the meanwhile, paquinimod (10 mg/kg) was injected via the intraperitoneal route for 10 days. (*A, B*) Body weight and colon length of FGF20 KO mice and WT mice with colitis, treated with paquinimod or vehicle. (*C*) Histologic morphology of FGF20 KO mice and WT mice with colitis, treated with paquinimod or vehicle. *Top*, H&E staining; *bottom*, PAS staining. Scale bar, 100 μm and 50 μm. (*D*) Immunoblot analysis of colonic IL6 and iNOS in FGF20 KO mice and WT mice with colitis, treated with paquinimod or vehicle (n = 6). Data are represented as mean $\pm$ SEM; *$P < .05$, ***$P < .001$.

showed inconsistent trends in the regulation of M2-like macrophage polarization-related gene mRNA levels (Figure 16*B* and *D*). Immunofluorescence staining was performed to further characterize the expression of CD86, a marker of M1-polarized macrophages/microglia. The immunofluorescence results showed that DSS treatment
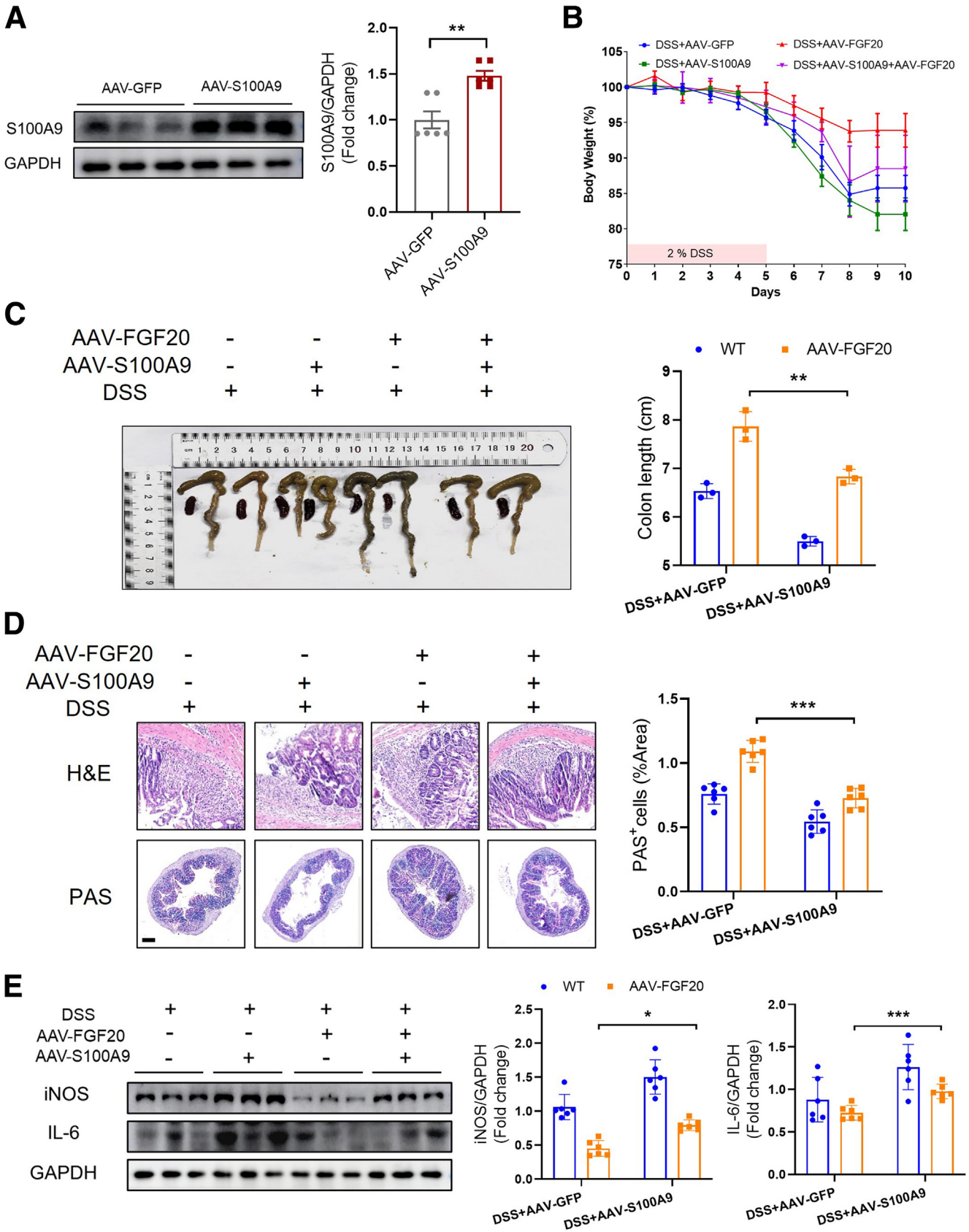
markedly upregulated CD86 expression in WT mice, which was further aggravated by FGF20 deficiency or S100A9 overexpression. In contrast, relief was observed with the inhibition of S100A9 or overexpression was FGF20 (Figure 16E and F). These results suggest that FGF20 inhibits M1-like macrophage polarization in colitis through the negative regulation of S100A9.

FGF20 Inhibits M1-like Macrophage Polarization through S100A9 in an NF-κB-Dependent Manner In Vivo and In Vitro

To date, several studies have shown that S1009A regulates NF-κB activity in various biologic processes, including tumorigenesis and colitis.[21] Consistently, our KEGG pathway analysis revealed considerable upregulation of the NF-κB signaling pathway in FGF20 KO mice following DSS administration compared with WT mice (Figure 17A). Immunoblotting further confirmed this finding, showing abnormal activation of NF-κB in DSS-treated FGF20 KO mice compared with WT mice (Figure 17B). In contrast, DSS-induced increases in colonic p-IκBα and p-p65 levels were notably reversed by paquinimod treatment in FGF20 KO mice (Figure 17C) and exacerbated by AAV-S100A9 treatment in AAV-FGF20 mice (Figure 17D).

Given these in vivo findings indicating that FGF20 modulates S100A9 signaling and suppresses M1-like macrophage polarization, we further investigated whether FGF20 regulates S100A9 expression via NF-κB signaling in primary peritoneal macrophages isolated from WT and FGF20 KO mice. In primary macrophages from WT mice stimulated with lipopolysaccharide (LPS), the expression of p-p65, p-IκBα, S100A9, and proinflammatory mediators, such as iNOS, TNF-α, and IL6, was considerably upregulated (Figure 18A). These effects were further exacerbated in primary macrophages derived from FGF20 KO mice (Figure 18A), consistent with the in vivo results. Notably, treatment with BAY11-7082, an NF-κB inhibitor, abolished the upregulation of p-p65, p-IκBα, iNOS, TNF-α, IL6, and S100A9 in primary macrophages from WT and FGF20 KO mice (Figure 18A). Furthermore, the expression of CD86, a marker of M1 polarization, was also evaluated by immunofluorescence staining. CD86 expression was markedly increased in LPS-treated primary macrophages from FGF20 KO mice compared with those from WT mice. However, BAY11-7082 markedly inhibited CD86 expression in primary macrophages derived from both LPS-treated FGF20 KO and WT mice (Figure 18B). These findings collectively suggest that FGF20 suppresses M1-like macrophage

polarization by negatively regulating S100A9 in an NF-κB-dependent manner.

Discussion

Although the protective effects of exogenous recombinant FGF20 protein in experimental models of intestinal inflammation have been reported, its exact molecular mechanism remains unclear. In the present study, we observed a marked increase in FGF20 levels in the inflamed colonic mucosa of patients with UC and mice with colitis. Consequently, we systematically investigated the mechanisms through which FGF20 contributes to UC pathogenesis. Our findings demonstrate that genetic deficiency of FGF20 markedly exacerbates colonic inflammation and impairs intestinal epithelial barrier integrity. These adverse effects were reversed by FGF20 supplementation. These results suggest that FGF20 upregulation in colitis represents a compensatory response to the inflammatory environment. Specifically, inflammatory signals in the gut seem to trigger increased expression of FGF20 as a protective mechanism aimed at mitigating tissue damage and promoting mucosal healing. This suggests that FGF20 functions as a physiological protector against UC. Consistent with this, studies have shown that elevated FGF10 acts as a compensatory mechanism against hepatic ischemia-reperfusion injury;[30] in contrast, our previous research demonstrated a similar role for FGF21 in combating atherosclerosis[31] and angiotensin II–induced hypertension.[32] In this study, we further revealed that FGF20 enhances intestinal epithelial barrier integrity and regulates the balance of colonic M1/M2 macrophage polarization through the modulation of S100A9. Elevated FGF20 levels in colonic tissue may suppress UC progression by inhibiting S100A9, M1 polarization, proinflammatory cytokine secretion, and inflammatory macrophage infiltration. Therefore, modulating FGF20 levels could be a novel therapeutic strategy for UC.

UC is a progressive disease characterized by chronic inflammation and impaired intestinal epithelial barrier integrity.[33] The immune response plays a crucial role in intestinal mucosal inflammation, making therapeutic strategies that target inflammatory cell activation and improve epithelial barrier integrity promising options for UC management.[34] During UC pathogenesis, proinflammatory mediators, such as iNOS, TNF-α, and IL6, are abundantly produced, exacerbating disease phenotypes, such as shortened colon length, reduced body weight, increased DAI, and disrupted tissue architecture.[35] In our study, these phenotypes were further aggravated in FGF20 KO mice compared with WT littermates (Figure 3). Notably, FGF20 overexpression

---

Figure 12. (*See previous page*). **AAV-S100A9 attenuates the protective effects of FGF20-overexpression against DSS-induced colitis.** Six-week-old male WT mice were treated with AAV-FGF20, AAV-S100A9, or AAV-GFP by tail vein injection. After 4 weeks of AAV injection, all mice were given 2% DSS in drinking water for 5 days, followed by normal drinking water for an additional 5 days. (A) The expression of S100A9 after AAV-S100A9 treatment was determined by Western blot (n = 6). (B, C) Body weights and colon length of AAV-FGF20-treated mice and AAV-GFP-treated mice with colitis, treated with AAV-S100A9 or not were measured. (D) Histologic morphology of AAV-FGF20-treated mice and AAV-GFP-treated mice with colitis, treated with AAV-S100A9 or not. *Top*, H&E staining; *bottom*, PAS staining. Scale bar, 100 μm and 50 μm. (E) Immunoblot analysis of colonic IL6 and iNOS in AAV-FGF20-treated mice and AAV-GFP-treated mice with colitis, treated with AAV-S100A9 or not (n = 6). Data are represented as mean ± SEM; *$P < .05$, **$P < .01$, ***$P < .001$.
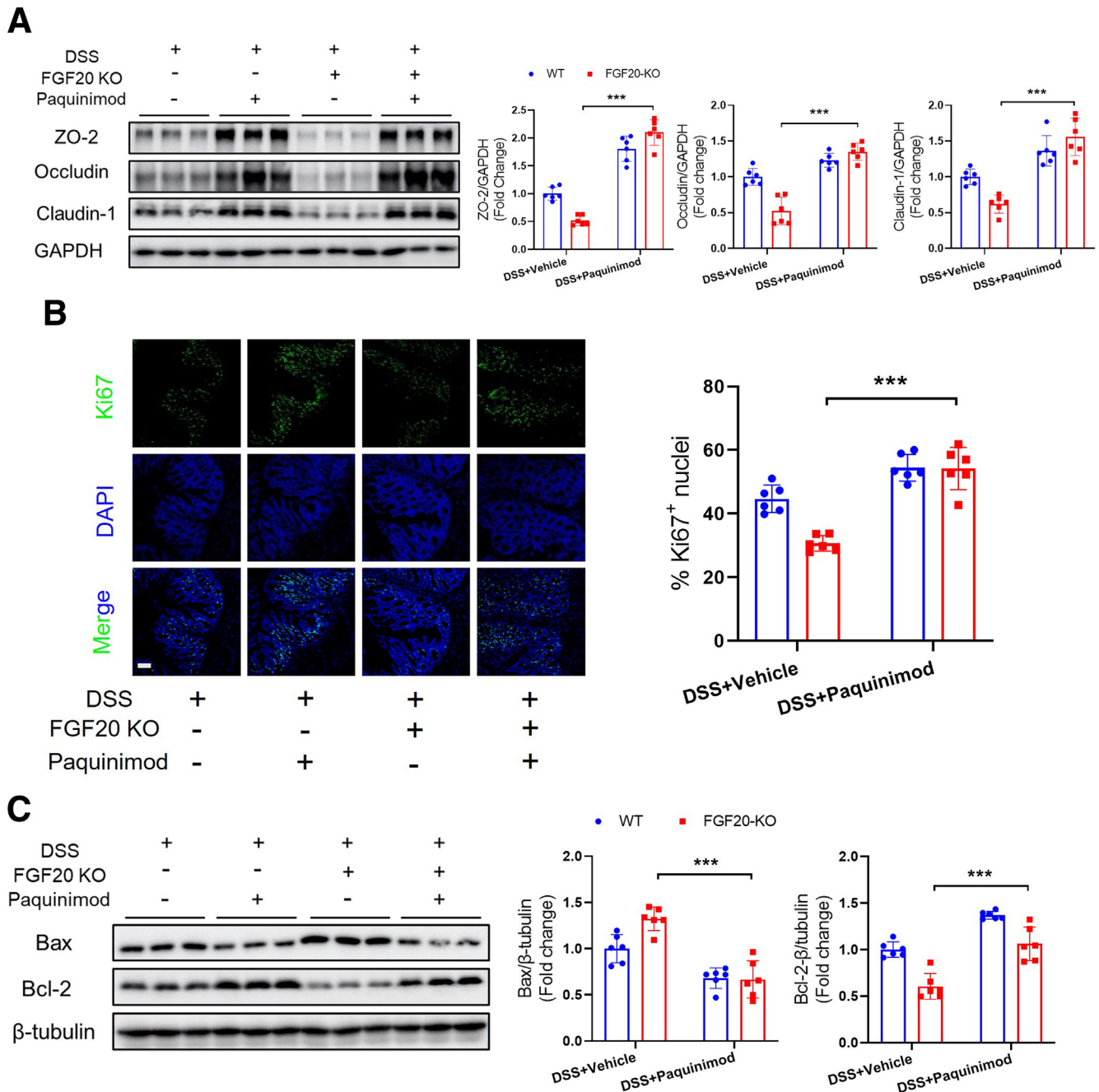
Figure 13. Inhibition of S100A9 mitigated the deterioration of FGF20 KO on intestinal barrier function in DSS-induced colitis. Eight-week-old male FGF20 KO mice and WT littermates were given 2% DSS in drinking water for 5 days, followed by normal drinking water for an additional 5 days. In the meanwhile, paquinimod (10 mg/kg) was injected via the intraperitoneal route for 10 days. (*A*) Western blot and quantitation of colonic ZO-2, occludin, and claudin 1 expression in FGF20 KO mice and WT mice with colitis, treated with paquinimod or vehicle (n = 6). (*B*) Representative fluorescence images of Ki67, and the percentage of Ki67-positive cells in FGF20 KO mice and WT mice with colitis, treated with paquinimod or vehicle. Scale bar, 50 μm (n $\geq$ 5). (*C*) Immunoblot analysis of colonic Bax and Bcl-2 expression in FGF20 KO mice and WT mice with colitis, treated with paquinimod or vehicle (n = 6). Data are represented as mean $\pm$ SEM; *P < .05, ***P < .001.

alleviated these adverse effects (Figure 4), demonstrating its ability to suppress excessive immune responses in colitis.

Intestinal epithelial barrier integrity, primarily supported by epithelial cell tight junctions, is essential for maintaining intestinal homeostasis and preventing harmful substances from entering the bloodstream.[36] Tight junctions, composed of transmembrane proteins, such as occludin, claudins, junction adhesion molecules, and associated cytoskeletal proteins, such as ZOs, regulate the selective permeability of the epithelial barrier.[37] Abnormal expression of tight junction proteins increases mucosal permeability, a hallmark of early IBD development and
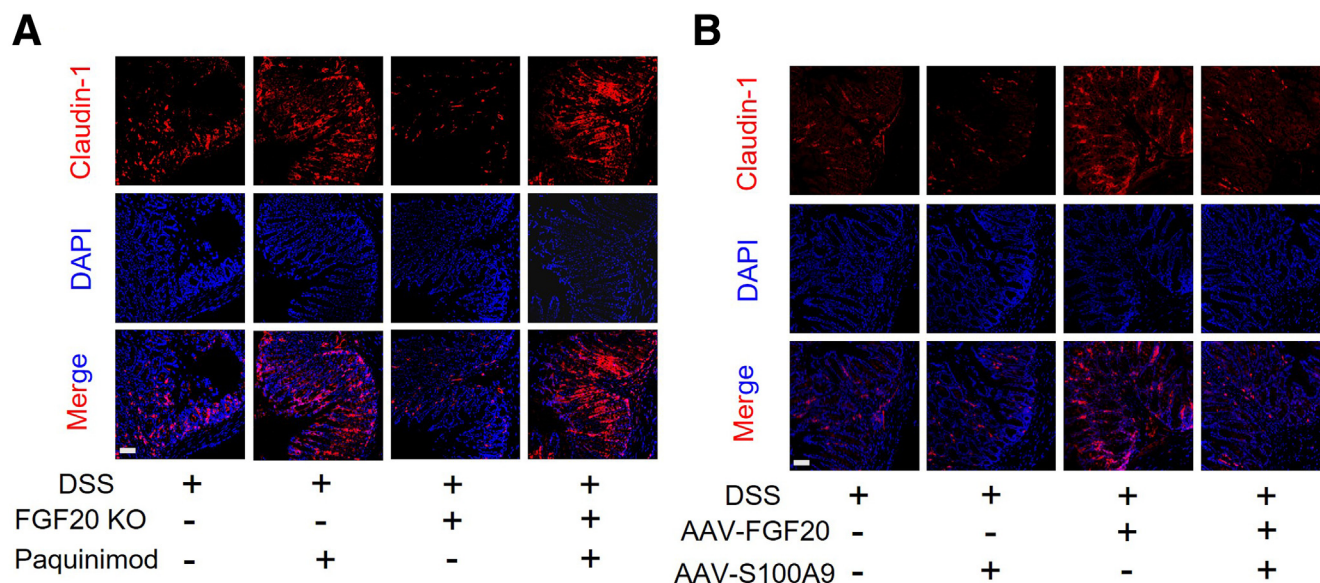
Figure 14. FGF20 regulates claudin-1 through S100A9 in DSS-induced colitis mice. (*A*) Representative fluorescence images of colonic claudin-1 from FGF20 KO mice and WT mice with colitis, treated with paquinimod or vehicle. (*B*) Representative fluorescence images of colonic claudin-1 from AAV-FGF20-treated mice and AAV-GFP-treated mice with colitis, treated with AAV-S100A9 or not. Scale bar, 50 μm.

recurrence.[38] Consistent with this, WT mice with colitis exhibited increased intestinal mucosal permeability, as evidenced by elevated FITC-dextran 4000 levels in the plasma. This permeability was further exacerbated in FGF20 KO mice (Figure 5*A*), along with marked downregulation of tight junction-related proteins, including ZO-2, occludin, and claudin-1 (Figures 5*B* and 6*A* and *B*). As envisioned, all these adverse effects induced by DSS on the intestinal epithelial barrier were reversed by AAV-FGF20 treatment (Figures 6*C* and *D* and 7*A*). Additionally, Hagiwara et al[39] reported a significantly higher apoptosis rate in intestinal epithelial cells from colonic biopsy samples of patients with active UC compared with healthy control subjects, suggesting that excess apoptosis surpasses the histiocyte capacity and contributes to epithelial defense breakdown and exacerbation of mucosal inflammation. These findings led us to hypothesize that FGF20's anticolitis effects stem not only from its ability to improve tight junction function but also from its regulation of intestinal epithelial cell proliferation and apoptosis. Supporting this, our immunofluorescence analysis for Ki67 demonstrated that FGF20 deficiency exacerbated DSS-reduced reductions in intestinal epithelial cell proliferation compared with WT littermates with colitis. A marked decrease in Ki67-positive cells reflected this effect (Figure 5*C*). AAV-FGF20 treatment alleviated the DSS-induced proliferation reduction (Figure 7*B*). Moreover, immunoblots revealed that FGF20 deficiency aggravated DSS-induced decreases in Bcl-2 expression and increases in Bax expression (Figure 5*D*), which were reversed by AAV-FGF20 treatment (Figure 7*C*). Collectively, these results indicate that FGF20 maintains intestinal barrier integrity by reinforcing tight junctions and promoting epithelial cell proliferation, thereby mitigating colitis.

Macrophages are pivotal in maintaining intestinal mucosal immune homeostasis.[40] Studies have linked macrophage infiltration into the colonic lamina propria with intestinal inflammation onset.[6] Similarly, excessive macrophage infiltration has been observed in colon tissues from patients with IBD and animal models, underscoring their role in both the initiation and resolution of inflammation.[30] In our study, we observed extensive immune cell infiltration, including macrophages, B cells, neutrophils, and CD4$^+$ T cells, in the colonic tissue of WT mice with colitis. This infiltration was further exacerbated in FGF20 KO mice (Figure 8), suggesting a connection between FGF20 and macrophage regulation. Macrophages exhibit plasticity and can polarize into proinflammatory M1 or anti-inflammatory M2 phenotypes, making them viable therapeutic targets for IBD. Disruption of M1/M2 polarization balance is a key factor influencing IBD outcomes.[41] Consistently, macrophage polarization in tissues of patients with IBD shows increased M1 markers (eg, CD86) and decreased M2 markers (eg, Arg1 and CD206).[42] This polarization shift[42] exacerbates inflammation and compromises intestinal barrier function. In FGF20 KO mice, colonic M1 polarization-related gene expression (eg, *IL-6*, *TNF-α*, *IL-1β*, and *MCP-1*) was considerably elevated (Figure 9*A*). These adverse effects were reversed by AAV-FGF20 treatment (Figure 9*C*). However, FGF20's effects on M2 polarization-related gene expression were inconsistent (Figure 9*B* and *D*). Together, current data suggest that FGF20 protection against DSS-induced colitis may be mediated, at least in part, by inhibiting M1 polarization.

S1009, a calcium-binding protein stored in neutrophils, monocytes, and macrophages,[43] is released during tissue injury or infection and plays a critical role in inflammation
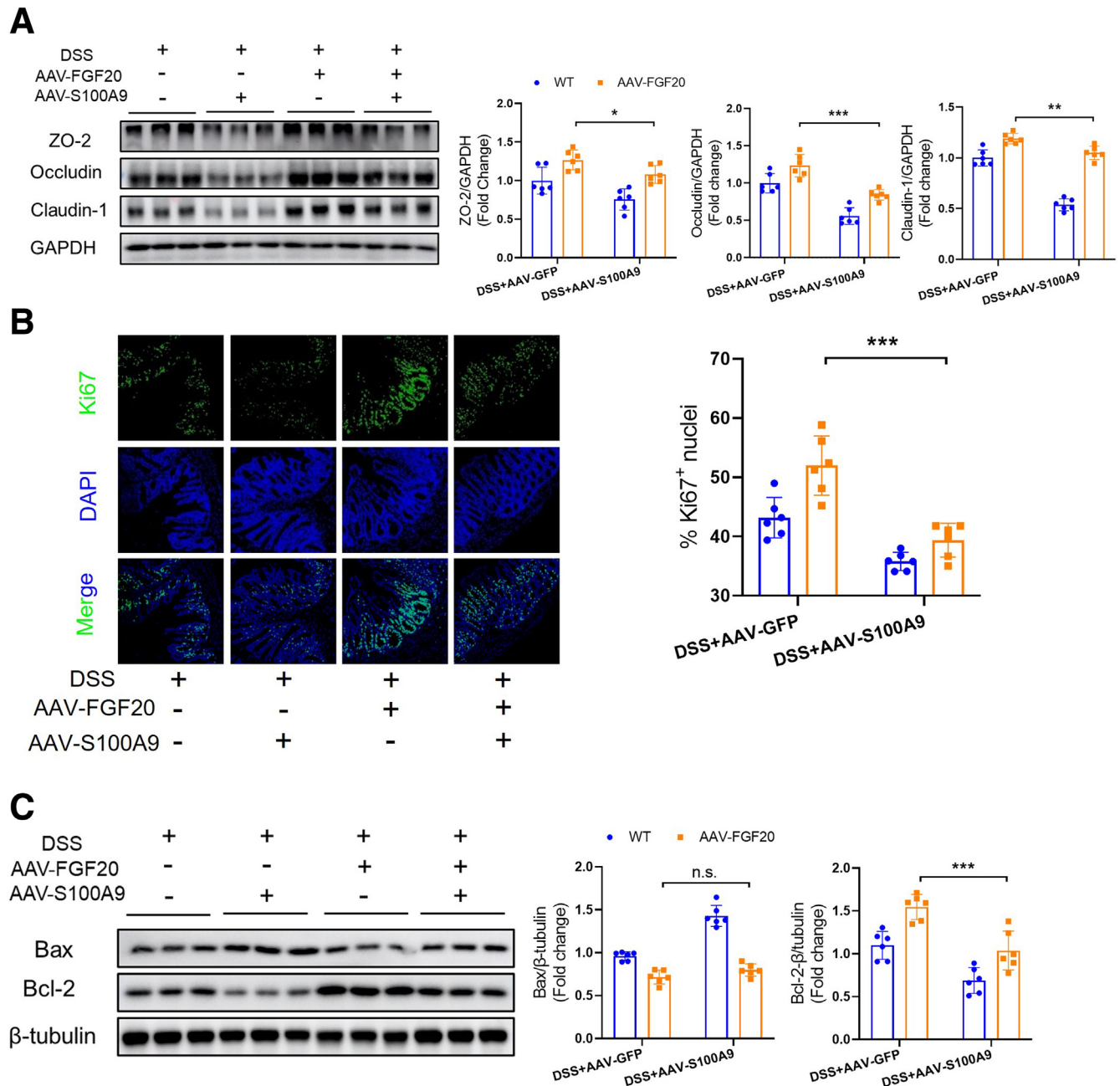
Figure 15. AAV-S100A9 abolished the protect effects of FGF20 overexpression on intestinal barrier function in DSS-induced colitis. Six-week-old male WT mice were treated with AAV-FGF20, AAV-S100A9, or AAV-GFP by tail vein injection. After 4 weeks of AAV injection, all mice were given 2% DSS in drinking water for 5 days, followed by normal drinking water for an additional 5 days. (*A*) Western blot and quantitation of colonic ZO-2, occludin, and claudin-1 expression in AAV-FGF20-treated mice and AAV-GFP-treated mice with colitis, treated with AAV-S100A9 or not (n = 6). (*B*) Representative fluorescence images of Ki67, and the percentage of Ki67-positive cells in AAV-FGF20-treated mice and AAV-GFP-treated mice with colitis, treated with AAV-S100A9 or not (n ≥ 5), Scale bar, 50 μm. (*C*) The expression of level of Bax and Bcl-2 in AAV-FGF20-treated mice and AAV-GFP-treated mice with colitis, treated with AAV-S100A9 or not, were detected by Western blot (n = 6). Data are represented as mean ± SEM; *$P < .05$, **$P < .01$, ***$P < .001$. n.s., no significance.

regulation. Elevated S100A9 levels are biomarkers for multiple inflammatory diseases, including IBD.[44] The pharmaceutic inhibition of S100A9 alleviates inflammation-related tissue injury and cell apoptosis.[19] Proteomic analysis in our study confirmed increased S100A9 levels in the

colonic tissue of DSS-treated WT mice, which were further elevated in DSS-induced FGF20 KO mice (Figure 10). These findings suggest that S100A9 is a key downstream target of FGF20 in colitis. Pharmacologic inhibition of S100A9 in FGF20 KO mice with colitis notably attenuated the
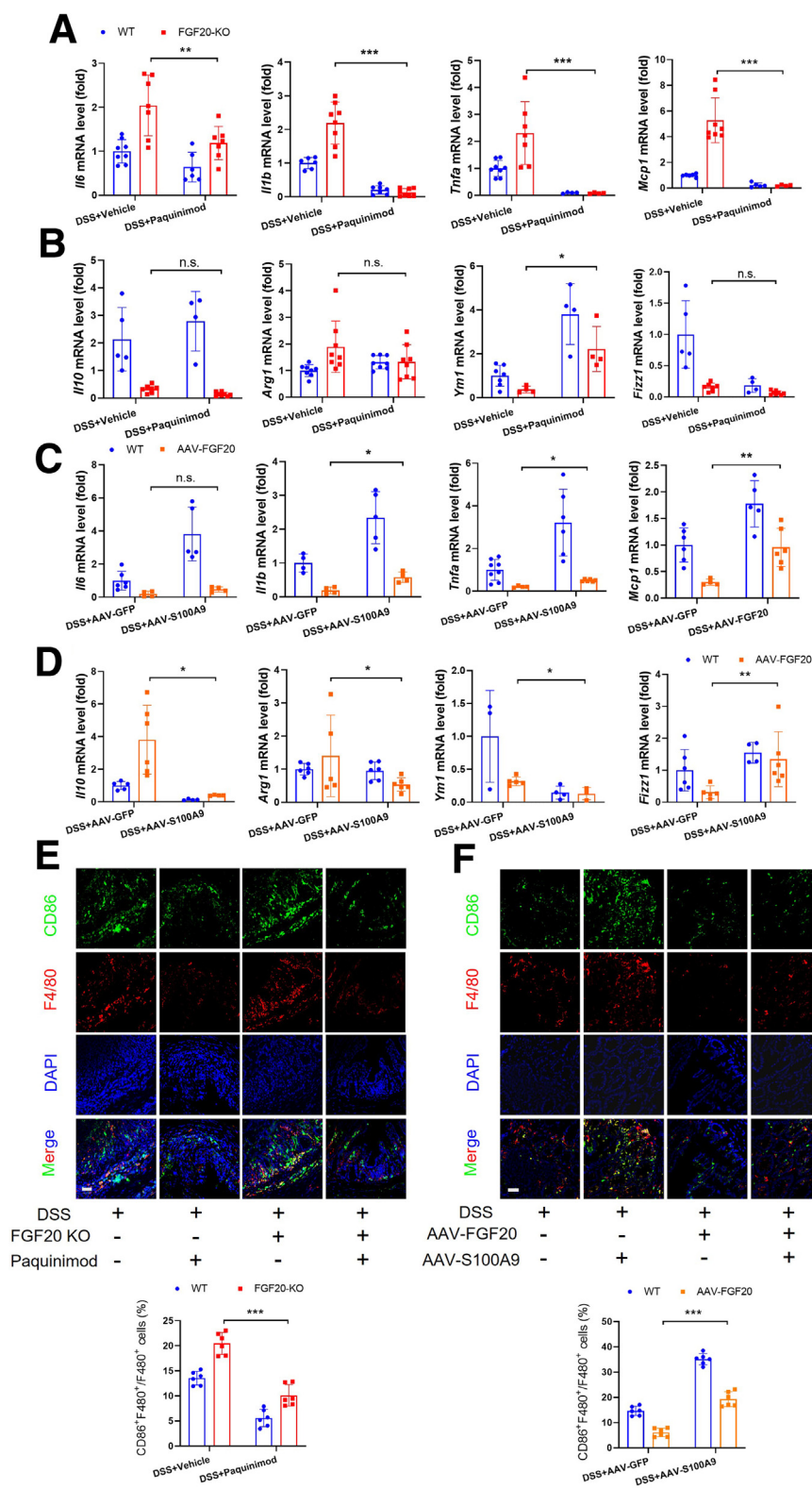
Figure 16. The inhibition of FGF20 on M1-like macrophage polarization in DSS-induced colitis was S100A9-dependent. (*A, B*) mRNA expression levels of macrophage M1 (*IL-6, TNF-α, IL-1β,* and *MCP-1*) and M2 (*IL-10, Arg-1, Fizz1,* and *Ym1*) polarization-related gene in FGF20 KO mice and WT mice with colitis, treated with paquinimod or vehicle, were quantitatively determined by quantitative PCR (n ≥ 4). (*C, D*) mRNA expression levels of macrophage M1 (*IL-6, TNF-α, IL-1β,* and *MCP-1*) and M2 (*IL-10, Arg-1, Fizz1,* and *Ym1*) polarization-related gene in AAV-FGF20-treated mice and AAV-GFP-treated mice with colitis, treated with AAV-S100A9 or not, were quantitatively determined by quantitative PCR (n ≥ 4). (*E*) Representative images of immunofluorescence staining of colon sections from FGF20 KO mice and WT mice with colitis, treated with paquinimod or vehicle. Scale bar, 50 μm. (*F*) Representative images of immunofluorescence staining of colon sections from AAV-FGF20-treated mice and AAV-GFP-treated mice with colitis, treated with AAV-S100A9 or not. Scale bar, 50 μm. Data are represented as mean ± SEM; *P < .05, **P < .01, ***P < .001. n.s., no significance.

exacerbated colitis phenotype and restored intestinal epithelial barrier integrity (Figures 11 and 13). Conversely, S100A9 overexpression attenuated the beneficial effect of FGF20 overexpression, reflected by worsened colitis and compromised barrier integrity in AAV-FGF20-treated mice with colitis (Figures 12 and 15). Prior studies have also linked S100A9 with macrophage polarization, specifically promoting M1 polarization and impairing macrophage differentiation.[45]
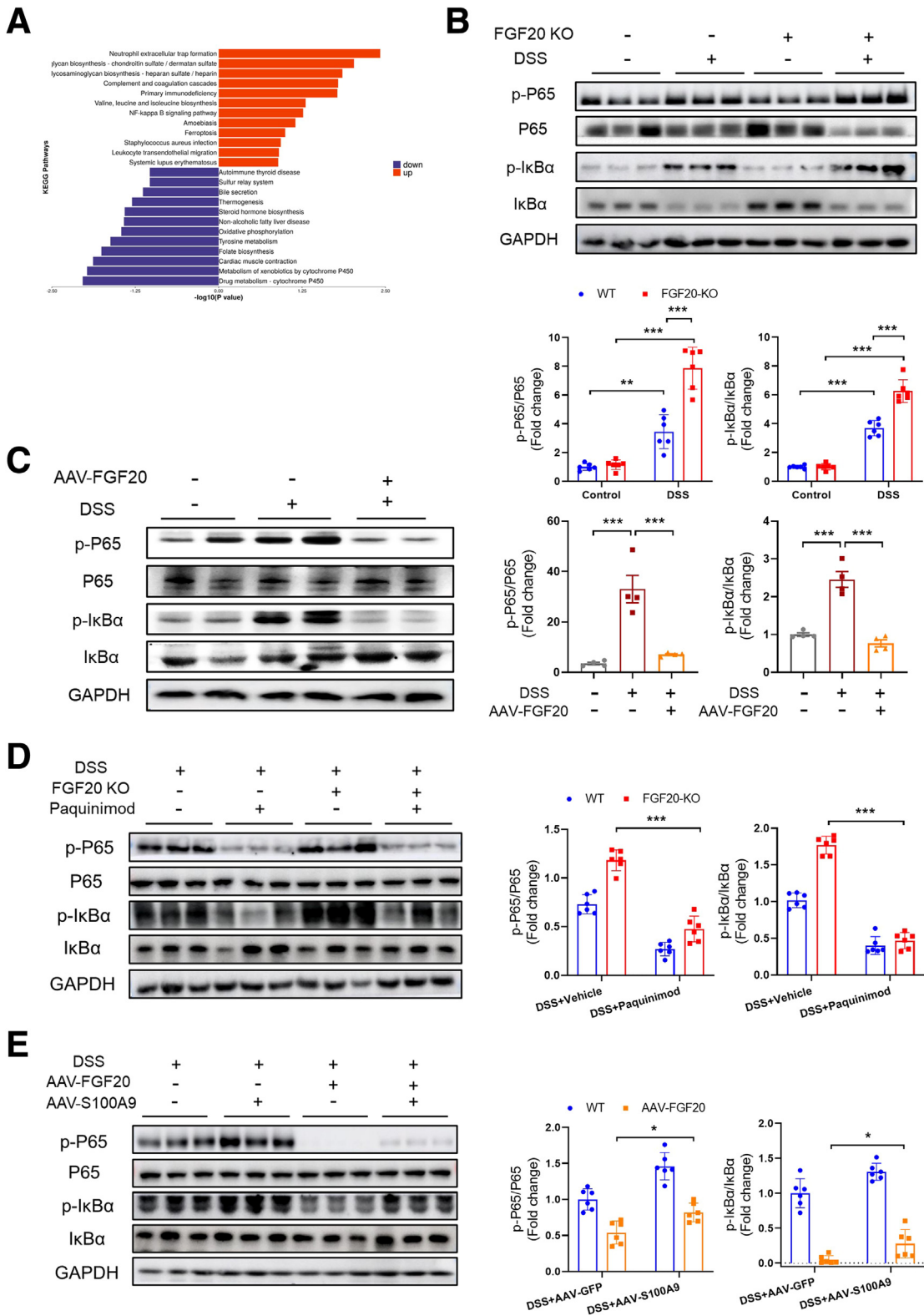
Figure 17. FGF20 inhibits NF-κB pathway through S100A9 in DDS-induced mice. (*A*) KEGG Enrichment Analysis of proteomics data from the colonic tissue of FGF20 KO and WT mice with or without colitis. (*B*) Immunoblot analysis of colonic p-P65, P65, p-IκBα, and IκBα from FGF20 KO and WT mice with or without colitis (n = 6). (*C*) Immunoblot analysis of colonic p-P65, P65, p-IκBα, and IκBα contents in AAV-FGF20- or AAV-GFP-treated mice with or without colitis. (*D*) Immunoblot analysis of colonic p-P65, P65, p-IκBα, and IκBα contents in FGF20 KO mice and WT mice with colitis, treated with paquinimod or vehicle (n = 6). (*E*) Immunoblot analysis of colonic p-P65, P65, p-IκBα, and IκBα contents in AAV-FGF20-treated mice and AAV-GFP-treated mice with colitis, treated with AAV-S100A9 or not (n = 6). Data are represented as mean ± SEM; *$P < .05$, **$P < .01$, ***$P < .001$.
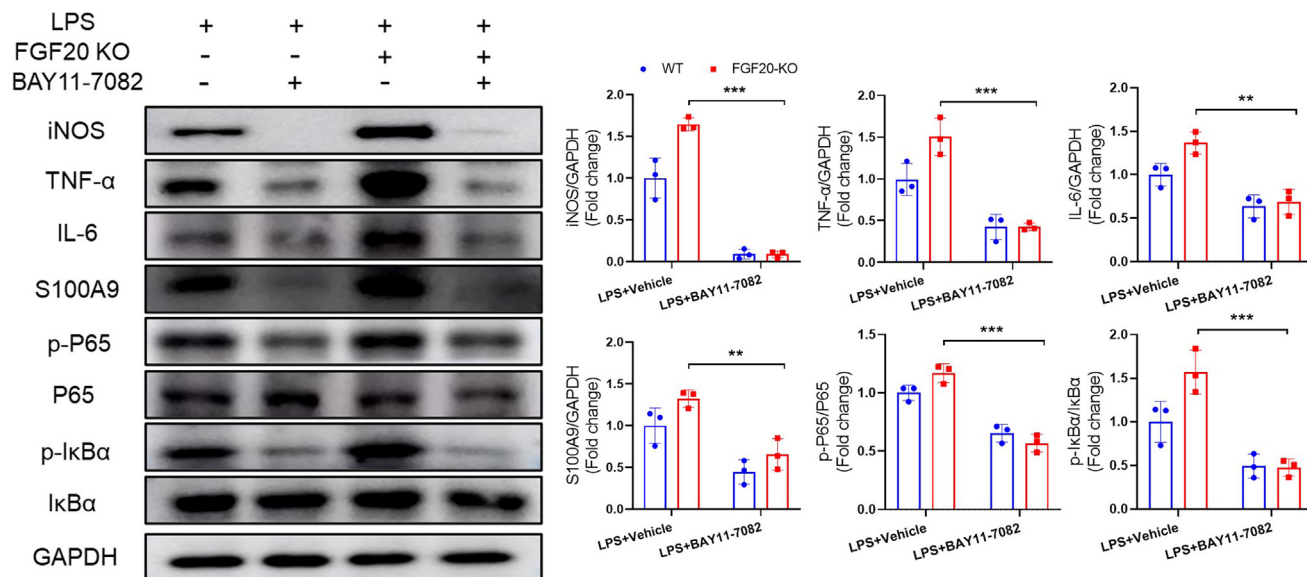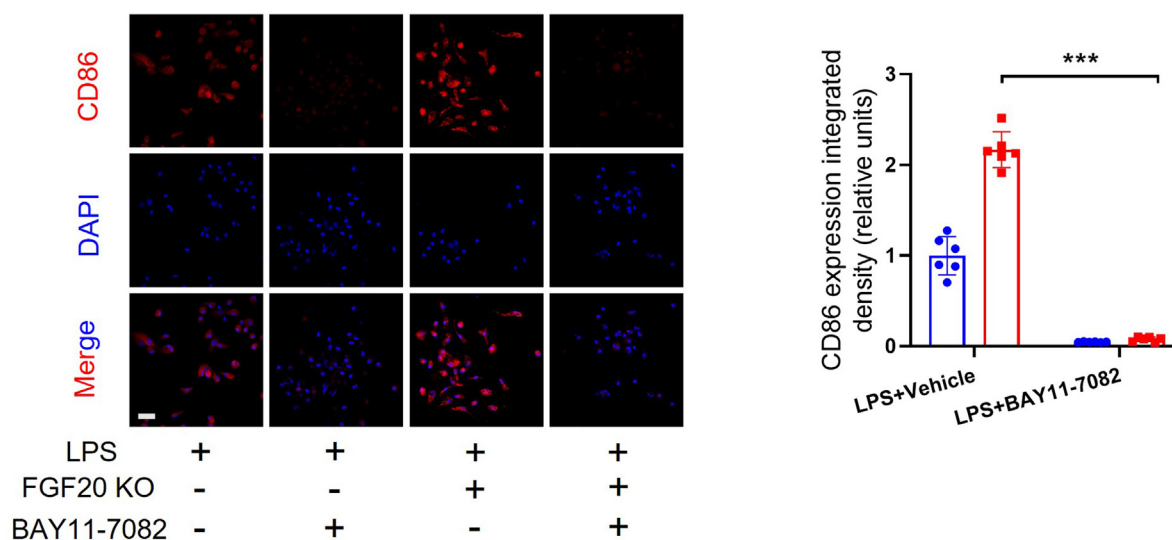
Figure 18. FGF20 inhibits M1-like macrophage polarization in NF-κB-dependent manner in vitro. Primary peritoneal macrophages were isolated from WT mice and FGF20 KO mice and used for subsequent in vitro experiments. (*A*) Immunoblot analysis of expression of iNOS, TNF-α, IL6, S100A9, p-P65, P65, p-IκBα, and IκBα in LPS-stimulated primary peritoneal macrophages, treated with or without BAY11-7082 (n = 3). (*B*) Representative immunofluorescence images and its fluorescence densities of LPS-stimulated primary peritoneal macrophages, treated with or without BAY11-7082 (n = 6). Data are represented as mean ± SEM; **P < .01, ***P < .001.

Consistently, S100A9 overexpression abolished FGF20's inhibitory effect on M1 polarization; in contrast, S100A9 inhibition reversed exacerbated M1 polarization in FGF20 KO mice (Figure 16). These findings indicate that S100A9 negatively regulates M1 polarization and intestinal barrier integrity in the context of FGF20-mediated colitis protection.

S100A9 is known to activate NF-κB, a pathway implicated in M1 polarization.[21] NF-κB signaling was enriched in KEGG pathway analysis of upregulated proteins in DSS-treated FGF20 KO mice (Figure 17A). Consistent with previous reports and our proteomics results, the in vivo data also confirmed that FGF20 overexpression inhibits NF-κB signaling; in contrast, FGF20 KO promotes its activation. These effects were further modulated by the replenishment of AAV-S100A9 and paquinimod, which abolished NF-κB activation in FGF20 KO mice (Figure 17). Additionally, in vitro experiments demonstrated considerably increased levels of proinflammatory mediators, including iNOS, TNF-α,

and IL6, in primary peritoneal macrophages isolated from FGF20 KO mice compared with those from WT mice after LPS treatment. These increases were fully suppressed by BAY11-7082, an NF-κB inhibitor (Figure 18). Interestingly, BAY11-7082 treatment also inhibited S100A9 expression in vitro, indicating a mutual regulatory relationship between S100A9 expression and NF-κB. M1 polarization, assessed via immunofluorescence staining of the marker CD86, was markedly inhibited by BAY11-7082 in primary peritoneal macrophages derived from both FGF20 KO and WT mice following LPS treatment (Figure 18). Collectively, these data suggest that FGF20 inhibits M1-like macrophage polarization through the negative regulation of S100A9 in an NF-κB-dependent manner.

In conclusion, this study uncovered the mechanisms underlying FGF20's protective effects in colitis. Specifically, FGF20 alleviates colitis by improving intestinal epithelial barrier integrity and inhibiting M1 polarization via the negative regulation of S100A9 in an NF-κB-dependent manner. These findings highlight FGF20 as a potential therapeutic target for UC, with the exogenous addition of recombinant FGF20 representing a promising treatment strategy for the disease.

Material and Methods
Animal Experiments

FGF20$^{+/-}$ mice were generated from Cyagen Biosciences Inc, Ltd. After heterozygous amplification with C57BL/6J WT mice, FGF20 heterozygous males and females were mated for several generations to obtain FGF20 KO pure-azygous mice and WT mice, which littered homozygous mice and WT mice were used for experiments. All mice were bred and maintained under specific pathogen-free conditions at the animal facility of the Wenzhou Medical University, with a 12-hour light cycle and given a regular chow diet and water ad libitum. Mice were used at 8–10 weeks of age and then were randomized each group for subsequent in vivo experiments. The UC mouse model was established following the previously described procedure with a slight modification.[46] Briefly, mice were given 2% DSS (molecular weight, 36,000–50,000 Da; MP Biomedicals, LLC, Solon, OH) in drinking water for 5 days, followed by normal drinking water for an additional 5 days. AAV were delivered to mice via tail vein injection. For the S100A9 inhibitor experiment, paquinimod (HY-100442, ABR 25757, MCE) was intraperitoneal injected to model group mice every day at a dose of 10 mg/kg, when they began to drink 2% DSS. The animal experiments conducted in this study received approval from the Animal Research Ethics Committee of Wenzhou Medical University.

Construction of AAV Vectors for Overexpression of FGF20 and S100A9

Recombinant AAV9 expressing FGF20 was provided by Wuhan Viral-Therapy Biotechnologies Co, Ltd. The amplification process involved the use of specific primers: 5'-AGGATCACAGTCTCTTCGGTATC-3' and 5'-GTCATTCATCC-CAAGGTACAGG-3'.Then DNA segment was inserted into the pAAV-IRES-ZsGreen plasmid to construct the pAAV-Mfgf20-IRES-ZsGreen vector. AAV9 expressing S100A9 was constructed and produced by Shanghai OBiO Technology Co, Ltd. The amplification process involved the use of specific primers: 5'-GGCAAAGGCTGTGGGAAGT-3' and 5'-CCATT-GAGTAAGCCATTCCCTTTA-3'. The DNA segment was inserted into the PAAV-CAG-MCS-3xFLAG-WPRE plasmid to construct the PAAV-CAG-S100a9-3xFLAG-WPRE vector. As the previously described,[47] AAV vectors were prepared using 3-plasmid transfection adenovirus-free protocol.

Histologic Analysis

Each group of the mice were monitored daily for the occurrence of weight change, diarrhea, and fecal bleeding to score the DAI.[48] Postmortem, the entire colon was removed and measured. The colon tissue was embedded in paraffin after fixed with 4% paraformaldehyde, and then sectioned and stained with hematoxylin & eosin (G1120, Solarbio, Beijing, China) and PAS (G1281, Solarbio). The changes in goblet cells in colon tissue were observed by AB-PAS staining. All images were captured using an optical microscope (BX53F2O, Olympus, Japan).

Immunofluorescence Staining

The colon sections were fixed with ice-cold ethanol for 20 minutes at -20°C and blocked with 5% bovine serum albumin at 37°C for 30 minutes. Then, the sections were covered with anti-F4/80 (1/500, GB11027-100, Servicebio, China), occludin (1/500, SC-133256, Santa Cruz), claudin-1 (1/500, SC-137121, Santa Cruz), and CD86 (1/500, 91882, CST) overnight at 4°C, and washed 3 times with phosphate-buffered saline (PBS) (pH7.0) for 5 minutes each time. The corresponding fluorescent secondary antibodies were then added for 60 minutes, washed with PBS 3 times for 5 minutes each time, and the sections were covered with DAPI (AB104139, Abcam, UK) for 20 minutes to visualize the nuclear DNA. The stained sections were observed using a positive fluorescence microscope. All immunofluorescence pictures were taken with a fluorescence microscope at the same exposure and intensity settings.

Enzyme-Linked Immunosorbent Assay Detection

Serum samples collected from mice were stored at -80°C before analysis. The serum FGF20 levels were measured using a commercially available enzyme-linked immunosorbent assay kit (abx389289, Abbexa, UK), according to the manufacturer's protocol.

Immunohistochemistry Staining

Paraffin sections of colon tissue were dewaxed and hydrated, and then antigen retrieval was performed. Tissue sections were washed thrice with PBS. Endogenous peroxidase activity was blocked by Envision Flex Peroxidase-Blocking Reagent (PV-9000, Zsgb-bio, China) for 30 minutes, followed by incubating with 5% (vol/vol) bovine serum albumin (10837091001, Roche, Switzerland) for 1 hour at room temperature. Tissue sections were incubated with F4/80 (1/500, GB113373-100, Servicebio), Ly6g (1/500, GB11229-100, Servicebio), CD4 (1/1000, ab183685,

Abcam), CD45 (1/100, BS79551, Bioworld, UK), and pAb (1:200) at 4°C overnight. Next day, sections were incubated with horseradish peroxidase–conjugated goat anti-IgG (1:400) at 37°C for 1 hour after washing thrice with PBS. Last, chromogenic reagent was achieved by DAB chromogenic reagent kit (ZLI-9018, Zhongshan Jinqiao Biotech Co, Ltd, China), and hematoxylin was further stained. The primary antibody of the negative control group was replaced with PBS. Finally, the slices were observed using a light microscope.

Western Blot Analysis

Colon tissues or cultured cells were lysed and centrifuged, and the protein concentration of supernatant was determined by Pierce BCA assay (23227, Thermo Scientific). Equal amounts (30 μg) of complete protein were subjected to 8%–12% sodium dodecyl sulfate-polyacrylamide gel electrophoresis gels and transferred onto 0.45-μm polyvinylidene fluoride membranes (Merck Millipore, Germany). After blocking with 5% skim milk for 1.5 hours, the membranes were incubated with respective primary antibodies at 4°C overnight. FGF20 (1/500, SC-373927, Santa CruzA), Bcl2 (1/1000, AB182858, Abcam), Bax (1/1000, AB32503, Abcam), S100A9 (1/500, SC-53187, Santa Cruz), S100A8 (1/500, SC-48352, Santa Cruz), phosphorylated (p) -IκBα (1/500, SC-8404, Santa Cruz), p-P65 (1/500, SC-136548, Santa Cruz), IκBα (1/1000, 4814S, CST, USA), P65 (1/1000, 4814S, CST), TNF-α (1/1000, AF7014, Affinity, China), IL6 (1/1000, 12912S, CST), FGFR1 (1/1000, bs-0230R, Bioss, China), FGFR2 (1/1000, bs-0675R, Bioss), FGFR3 (1/2000, MA5-31142, ThermoFisher), FGFR4 (1/1000, bsm-61509R, Bioss), GAPDH (1/10000, HRP-60004, Proteintech, China), and Beta-Tubulin (1/5000, 10094-1-AP, Proteintech). Membranes were washed and followed by incubation with corresponding secondary antibodies. Specific protein bands were visualized by exposure machine (Amersham Image Quant 800, GE) using enhanced-chemiluminescent substrate (K-12045-D50, Advansta) and quantitatively processed with Image J software.

Real-Time Quantitative Polymerase Chain Reaction Assay

Total RNA was extracted from colonic tissue by the Trizol reagent (15596018, Invitrogen). RNA was reverse transcribed using Improm-II reverse transcription kit (A5001, Promega) for quantitative PCR. The specific primers are described in Table 1. Target gene expression was normalized against GAPDH gene expression level.

Intestinal Permeability Assay

Intestinal permeability was evaluated using FITC-dextran with an average molecular weight of 3000–5000 (FD4-250 mg, Sigma-Aldrich). Briefly, mice were starved for 4 hours and then gavaged with FITC-dextran. After 4 hours, blood was collected via retro-orbital bleeding and centrifuged at 12,000 g for 3 minutes. A Spark multimode microplate reader (Tecan, Tecan Trading AG, Switzerland) was used for detecting the fluorescent intensity (excitation, 490 nm; emission, 528 nm). Each sample was measured in triplicate.

Primary Peritoneal Macrophages Extraction, Culture, and Stimulation

Primary peritoneal macrophages were obtained by peritoneal lavage 3 days after intraperitoneal injection (3 mL) of sterile 3% thioglycolate broth in WT mice and FGF20-KO mice. Washed cells were resuspended in RPMI 1640 medium that contained 2% fetal bovine serum, 1% penicillin/streptomycin, and 2-mm l-glutamine. After plating, cells were incubated overnight at 37°C and then washed with PBS to remove nonadherent cells. We pretreated the macrophage cells with a widely used NF-κB inhibitor, BAY 11-7082 (HY-13453, MCE;1 μM/mL), before LPS (L2630-10MG, Sigma-Aldrich; 0.5 μM/mL) sustainably stimulation to activate M1 polarization.

GEO Dataset Analysis

All microarray data were downloaded from the GEO database (http://www.ncbi.nih.gov/geo). The raw data were downloaded as MINiML files. It contains the data for

Table 1. Primers Used for the Real-Time Quantitative PCR Assays in this Study

Gene	Forward primers (5'-3')	Reverse primers (5'- 3')
FGF20	AGGATCACAGTCTCTTCGGTATC	GTCATTCATCCCAAGGTACAGG
TNF-α	AGCCCATGTTGTAGCAAACC	CCAAAGTAGACCTGCCCAGA
IL6	TGAACTCCTTCTCCACAAGC	ATCCAGATTGGAAGCATCCA
IL-1β	GGACAGAATATCAACCAACAAGTGATA	GTGTGCCGTCTTTCATTACACAG
IL10	AAGGGGTTACTTGGGGTTGCCA	AAATCGATGACAGCGTCGCA
YM1	TTCTTGTCACAGGTCTGG	CCTTAGCCCAACTGGTATAGT
ARG1	TGCAGTGGCAGAAATCAAGA	AGCATCCACCCAAATGACA
FIZZL1	CAGGATGCCAACTTTGAATAGG	CACAAGCACACCCAGTAGCAGTC
MCP-1	GAATCTGGAACATTCTGTGCTGTCC	GAATCTGGAACATTCTGTGCTGTCC
INOS	CCCCTGGAAGTTTCTCTTCAAAGTC	GAATCTGGAACATTCTGTGCTGTCC
GAPDH	TGACAACTCCCTCAAGATTGTCA	GGCATGGACTGTGGTCATGA

all platforms, samples, and GSE records of the GSE. The extracted data were normalized by log2 transformation. The microarray data were normalized by the normalize quantiles function of the preprocessCore package in R software (version 3.4.1). Probes were converted to gene symbols according to the annotation information of the normalized data in the platform. Probes matching multiple genes were removed from these datasets. The average expression value of gene measured by multiple probes was calculated as the final expression value. As in the case of the same dataset and platform but in different batches, the removeBatchEffect function of the limma package in the R software was used to remove batch effects. As in different datasets or in the same dataset but in different platforms, extracting multiple data sets with common gene symbols, and marking different datasets or different platforms as different batches, the removeBatchEffect function of the limma package in the R software was used to remove batch effects. The result of the data preprocessing was assessmented by boxplot. The PCA plot was drawn to illustrate the samples before and after batch effect.

Statistics

Data are presented as the mean $\pm$ standard error of the mean and were performed using GraphPad Prism 8.0 software (GraphPad Software, San Diego, CA). For data with normal distribution, a 2-tailed unpaired Student t test (2 groups) was used and presented as mean $\pm$ standard error of the mean, or Mann-Whitney test for nonnormal data (2 groups), or 1-way or 2-way analysis of variance followed by Tukey multiple comparisons posttest ($>$2 groups) was applied. Values of $P<.05$ were considered statistically significant.

References

1. Le Berre C, Honap S, Peyrin-Biroulet L. Ulcerative colitis. Lancet 2023;402:571–584.
2. Guan Q. A comprehensive review and update on the pathogenesis of inflammatory bowel disease. J Immunol Res 2019;2019:7247238.
3. Atreya R, Neurath MF. The sphingosine-1-phosphate receptor agonist etrasimod in ulcerative colitis. Lancet 2023;401:1132–1133.
4. Sheng YH, Davies JM, Wang R, et al. MUC1-mediated macrophage activation promotes colitis-associated colorectal cancer via activating the interleukin-6/signal transducer and activator of transcription 3 axis. Cell Mol Gastroenterol Hepatol 2022;14:789–811.
5. Wang K, Xu R, Snider AJ, et al. Alkaline ceramidase 3 deficiency aggravates colitis and colitis-associated tumorigenesis in mice by hyperactivating the innate immune system. Cell Death Dis 2016;7:e2124.
6. Yang H, Mirsepasi-Lauridsen HC, Struve C, et al. Ulcerative colitis-associated *E. Coli* pathobionts potentiate colitis in susceptible hosts. Gut Microbes 2020;12:1847976.
7. Garrido-Trigo A, Corraliza AM, Veny M, et al. Macrophage and neutrophil heterogeneity at single-cell spatial resolution in human inflammatory bowel disease. Nat Commun 2023;14:4506.
8. Zheng X, Jiang Q, Han M, et al. FBXO38 regulates macrophage polarization to control the development of cancer and colitis. Cell Mol Immunol 2023; 20:1367–1378.
9. Huang C, Wang J, Liu H, et al. Ketone body beta-hydroxybutyrate ameliorates colitis by promoting M2 macrophage polarization through the STAT6-dependent signaling pathway. BMC Med 2022;20:148.
10. Jinfeng L, Yunliang W, Xinshan L, et al. The effect of MSCs derived from the human umbilical cord transduced by fibroblast growth factor-20 on Parkinson's disease. Stem Cells Int 2016;2016:5016768.
11. Boshoff EL, Fletcher E, Duty S. Fibroblast growth factor 20 is protective towards dopaminergic neurons in vivo in a paracrine manner. Neuropharmacology 2018; 137:156–163.
12. Chen Y, An N, Zhou X, et al. Fibroblast growth factor 20 attenuates pathological cardiac hypertrophy by activating the SIRT1 signaling pathway. Cell Death Dis 2022; 13:276.
13. Whitehead GG, Makino S, Lien CL, et al. Fgf20 is essential for initiating zebrafish fin regeneration. Science 2005;310:1957–1960.
14. Alvarez E, Fey EG, Valax P, et al. Preclinical characterization of CG53135 (FGF-20) in radiation and concomitant chemotherapy/radiation-induced oral mucositis. Clin Cancer Res 2003;9:3454–3461.
15. Schuster MW, Shore TB, Harpel JG, et al. Safety and tolerability of velafermin (CG53135-05) in patients receiving high-dose chemotherapy and autologous peripheral blood stem cell transplant. Support Care Cancer 2008;16:477–483.
16. Chen J, Wang X, Hu J, et al. FGF20 Protected against BBB disruption after traumatic brain injury by upregulating junction protein expression and inhibiting the inflammatory response. Front Pharmacol 2020;11:590669.
17. Guo R, Wang X, Fang Y, et al. RhFGF20 promotes angiogenesis and vascular repair following traumatic brain injury by regulating Wnt/beta-catenin pathway. Biomed Pharmacother 2021;143:112200.
18. Jeffers M, Mcdonald WF, Chillakuru RA, et al. A novel human fibroblast growth factor treats experimental intestinal inflammation. Gastroenterology 2002;123:1151–1162.
19. Gong C, Ma J, Deng Y, et al. S100a9(-/-) alleviates LPS-induced acute lung injury by regulating M1 macrophage polarization and inhibiting pyroptosis via the TLR4/MyD88/NFkappaB signaling axis. Biomed Pharmacother 2024;172:116233.
20. Hanel A, Carlberg C. Time-resolved gene expression analysis monitors the regulation of inflammatory mediators and attenuation of adaptive immune response by vitamin D. Int J Mol Sci 2022;23:911.
21. Olsson A, Nakhle J, Sundstedt A, et al. Tasquinimod triggers an early change in the polarization of tumor associated macrophages in the tumor microenvironment. J Immunother Cancer 2015;3:53.
22. Mu S, Xiang H, Wang Y, et al. The pathogens of secondary infection in septic patients share a similar genotype to those that predominate in the gut. Crit Care 2022; 26:68.

23. Le N, Mazahery C, Nguyen K, et al. Regulation of intestinal epithelial barrier and immune function by activated T cells. Cell Mol Gastroenterol Hepatol 2021;11:55–76.

24. Yang J, Pei G, Sun X, et al. RhoB affects colitis through modulating cell signaling and intestinal microbiome. Microbiome 2022;10:149.

25. Ma Y, Yue J, Zhang Y, et al. ACF7 regulates inflammatory colitis and intestinal wound response by orchestrating tight junction dynamics. Nat Commun 2017;8:15375.

26. Na YR, Jung D, Stakenborg M, et al. Prostaglandin E (2) receptor PTGER4-expressing macrophages promote intestinal epithelial barrier regeneration upon inflammation. Gut 2021;70:2249–2260.

27. Lin Y, Yang X, Yue W, et al. Chemerin aggravates DSS-induced colitis by suppressing M2 macrophage polarization. Cell Mol Immunol 2014;11:355–366.

28. Wang S, Song R, Wang Z, et al. S100a8/a9 in inflammation. Front Immunol 2018;9:1298.

29. Silvin A, Chapuis N, Dunsmore G, et al. Elevated calprotectin and abnormal myeloid cell subsets discriminate severe from mild COVID-19. Cell 2020;182:1401–1418.

30. Li S, Zhu Z, Xue M, et al. The protective effects of fibroblast growth factor 10 against hepatic ischemia-reperfusion injury in mice. Redox Biol 2021;40:101859.

31. Lin Z, Pan X, Wu F, et al. Fibroblast growth factor 21 prevents atherosclerosis by suppression of hepatic sterol regulatory element-binding protein-2 and induction of adiponectin in mice. Circulation 2015;131:1861–1871.

32. Pan X, Shao Y, Wu F, et al. FGF21 Prevents angiotensin II-induced hypertension and vascular dysfunction by activation of ACE2/angiotensin-(1-7) axis in mice. Cell Metab 2018;27:1323–1337.

33. Na YR, Stakenborg M, Seok SH, et al. Macrophages in intestinal inflammation and resolution: a potential therapeutic target in IBD. Nat Rev Gastroenterol Hepatol 2019;16:531–543.

34. Sun Q, Li S, Lin R, et al. HUC-MSCs therapy for Crohn's disease: efficacy in TNBS-induced colitis in rats and pilot clinical study. EBioMedicine 2024;103:105128.

35. Lee Y, Kim SH, Jeong H, et al. Role of Nox4 in mitigating inflammation and fibrosis in dextran sulfate sodium-induced colitis. Cell Mol Gastroenterol Hepatol 2023;16:411–429.

36. Wang C, Wei S, Liu B, et al. Maternal consumption of a fermented diet protects offspring against intestinal inflammation by regulating the gut microbiota. Gut Microbes 2022;14:2057779.

37. Chen Z, Hao W, Gao C, et al. A polyphenol-assisted IL-10 mRNA delivery system for ulcerative colitis. Acta Pharm Sin B 2022;12:3367–3382.

38. Lee YS, Wollam J, Olefsky JM. An integrated view of immunometabolism. Cell 2018;172:22–40.

39. Hagiwara C, Tanaka M, Kudo H. Increase in colorectal epithelial apoptotic cells in patients with ulcerative colitis ultimately requiring surgery. J Gastroenterol Hepatol 2002;17:758–764.

40. Liu L, Wu Y, Wang B, et al. DA-DRD5 signaling controls colitis by regulating colonic M1/M2 macrophage polarization. Cell Death Dis 2021;12:500.

41. Mao Q, Pan H, Zhang Y, et al. GelNB molecular coating as a biophysical barrier to isolate intestinal irritating metabolites and regulate intestinal microbial homeostasis in the treatment of inflammatory bowel disease. Bioact Mater 2023;19:251–267.

42. Spalinger MR, Sayoc-Becerra A, Santos AN, et al. PTPN2 regulates interactions between macrophages and intestinal epithelial cells to promote intestinal barrier function. Gastroenterology 2020;159:1763–1777.

43. Jiang H, Zhao Y, Su M, et al. A proteome-wide screen identifies the calcium binding proteins, S100a8/S100a9, as clinically relevant therapeutic targets in aortic dissection. Pharmacol Res 2024;199:107029.

44. Pruenster M, Vogl T, Roth J, et al. S100a8/a9: from basic science to clinical application. Pharmacol Ther 2016; 167:120–131.

45. Franz S, Ertel A, Engel KM, et al. Overexpression of S100a9 in obesity impairs macrophage differentiation via TLR4-NFkB-signaling worsening inflammation and wound healing. Theranostics 2022;12:1659–1682.

46. Yu W, Wang G, Lu C, et al. Pharmacological mechanism of Shenlingbaizhu formula against experimental colitis. Phytomedicine 2022;98:153961.

47. Ito T, Okada T, Mimuro J, et al. Adenoassociated virus-mediated prostacyclin synthase expression prevents pulmonary arterial hypertension in rats. Hypertension 2007;50:531–536.

48. Vlantis K, Polykratis A, Welz PS, et al. TLR-independent anti-inflammatory function of intestinal epithelial TRAF6 signalling prevents DSS-induced colitis in mice. Gut 2016;65:935–943.

Correspondence
Address correspondence to: Fan Wu, PhD, The Affiliated Dongguan Songshan Lake Central Hospital, Guangdong Medical University, No. 7 Xianglong Road, Dongguan, 523326, Guangdong, PR China. e-mail: zflwf@126.com; or Zhuofeng Lin, PhD, The Affiliated Dongguan Songshan Lake Central Hospital, Guangdong Medical University, No. 7 Xianglong Road, Dongguan, 523326, Guangdong, PR China. e-mail: zlin@gdmu.edu.cn.